PbS-CdS Thin Film Heterojunctions for Photovoltaic Applications

A thesis submitted
in partial fulfillment of the requirements for
the award of degree of

Masters of Technology
in
Materials and Metallurgical Engineering

Submitted by
KRIPAL SINGH
Reg. No. 601202007

Under the guidance of
Dr. Bhaskar Chandra Mohanty
Assistant Professor
School of Physics and Materials Science

School of Physics and Materials Science
Thapar University
(Established under section 3 of UGC Act, 1956)
Patiala -147001, India

CERTIFICATE

This is to certify that the thesis entitled **"PbS - CdS Thin Film Heterojunctions for Photovoltaic Applications"** submitted by **Kripal Singh, Roll no. 601202007** in the partial fulfillment of the requirement for the award of the degree **M. Tech.** in **Materials and Metallurgical Engineering** from the School of Physics and Materials Science, Thapar University, Patiala, is a record of candidate's own work carried out by him under my supervision and guidance. The matter embodied in this report has not been submitted in part or full to any other university or institute for the award of any degree.

(Dr. B. C. Mohanty) 2/6/2014
Assistant Professor
School of Physics and Material Science
Thapar University, Patiala-147004 (Punjab)

Countersigned by:

(Dr. Kulvir Singh)
Professor & Head,
School of Physics and Material Science,
Patiala-147004 (Punjab)

(Dr. S. K. Mohapatra)
Dean Academic Affairs,
Thapar University,
Patiala-147004 (Punjab)

Dated:

I dedicate my thesis work
to the soldiers of my country
who sacrifice their lives

DECLARATION

I hereby declare that the work being presented in this thesis report entitled **"PbS-CdS Thin Film Heterojunctions for Photovoltaic Applications"** by me in partial fulfillment of the requirements of the award of degree of **Master of Technology** in **Materials Science and Engineering** from **School of Physics and Materials Science**, Thapar University, Patiala is an authentic record of my work carried out under the supervision of **Dr. Bhaskar Chandra Mohanty, Assistant Professor, School of Physics and Materials Science, Thapar University**. The matter presented in this report has not been submitted in any other University/Institute for the award of Masters of Technology or any other degree.

Kripal Singh

Reg. No. 601202007

ACKNOWLEDGEMENTS

I would like to express my deep sense of gratitude to Dr. B.C. Mohanty, *Assistant Professor School of Physics and Materials Science, Thapar University, Patiala* for his invaluable suggestion, excellent supervision, constant encouragement, thought provoking and unabashed discussion in nurturing the work and during the preparation of manuscript throughout the research work.

My sincere thanks to Dr. Kulvir Singh, *Professor and Head, School of Physics and Materials Science, Thapar University, Patiala* and Dr. S.K. Mohapatra, *Dean of Academic Affairs, Thapar University, Patiala* for providing me with the opportunity to conduct this work and bring it out in the present form.

I offer special thanks and regards to Ms. Indu Gupta, Ms. Parveer Kaur, Mr. Satwinder Singh and Ms. Chandani Rana, *Research Scholars, School of Physics and Materials Science, Thapar University,* Patiala for providing immense support in performing, characterizing and evaluating the thesis work.

I would also like to thank my friends (Gaganjot, Bharat Bhushan) for their kind support and encouragement.

I take my opportunity to express my heartfelt adulation to Prof. Yong Soo Cho and his group at Yonsei University, Seoul, South Korea for their help in characterizing some of my samples.

The greatest thanks go to my family members for their infinite support at each and every part of my life. Above all, I express my indebtedness to the almighty for all his blessing and kindness.

Kripal Singh

Reg. No. 601202007

ABSTRACT

Lead Sulfide (PbS) and Cadmium Sulfide (CdS) thin films were grown on the glass and indium tin oxide (ITO) coated substrates by chemical bath deposition (CBD) process. Lead acetate, cadmium chloride and thiourea were used in aqueous solutions as the ion sources of Pb, Cd and S. Films were grown for different durations ranging from 30 to 180 min at bath temperatures in the range of 30 to 80 °C to determine the optimum film quality suitable for photovoltaic applications. The properties of the resulting thin films were characterized by various techniques such as X-ray diffraction (XRD), scanning electron microscopy (SEM), atomic force microscopy (AFM) and optical absorption measurements. Photovoltaic response was studied by fabricating Schottky (ITO/PbS/Al) and heterojunctions (ITO/CdS/PbS/Al) structures. It was found that at a low temperature of 30 °C, it was not possible to grow the films irrespective of the deposition time. For the PbS films, deposition at 40 and 60°C yielded films characterized by numerous holes for deposition times as long as 180 min, and hence, no photovoltaic response from those samples could be obtained. At 80 °C, the films were dense, of polycrtsalline nature and showed a band gap of 1.4 to 1.6 eV, the most preferred one for the photovoltaic applications. Compared to PbS, the rate of dissociation of reagent compounds in the solution and formation of the compound on the substrate is faster for CdS for similar bath temperature. The band gap of the CdS films for a deposition time ranging from 30 to 160 min was in the range of 2.3 to 2.6 eV. From the current density – voltage curves of the fabricated heterojunction of the structure ITO/CdS/PbS/Al,very poor photovoltaic response was observed, possibly due to inferior film and interface properties.

CONTENTS

LIST OF TABLES

LIST OF FIGURES

CHAPTER 1

INTRODUCTION

Thin solid films are crystalline or non-crystalline solid materials developed two dimensionally on a substrate surface and are bound by two interfaces, namely at film-substrate and at film-ambient. The atoms at the interfaces are different from the atoms in the bulk in view of their surrounding and forces which arise due to termination of the material. The macroscopic properties of the bulk materials largely depend on the number of atoms present in the material and are not altered by a small fraction of atoms at the surface/interfaces. However, as the thickness decreases or the surface to volume ratio increases, the interfaces assume higher significance and in fact, provide thin films with properties, which are very different from those of their bulk counterparts. This has been capitalized to technological advantage, and consequently, thin films have been widely studied, both theoretically and experimentally, over the years. They have been adapted to fulfill a wide variety of functions and have been used in applications as diverse as electronics, energy harvesting systems, bio-mechanics, corrosion resistance and protection, decoration, magnetic coatings, data storage, etc. It has been found that the progress in each of these fields has depended on how quickly and efficiently films with new or improved properties could be developed through a cost-balanced and more reliable technology for industrial production. For instance, in the last few decades, progress in the thin film deposition techniques has led to strides in miniaturization of electronics components and circuits, which has been manifested by the explosive growth in communication and information processing, storage, and display applications [1].

In the recent years, thin films are being extensively studied for their potential applications in photovoltaic (PV) technology. The PV has emerged as an alternate key technology following the serious environmental threat stemming from fossil fuel combustion for energy solutions of the human race. The PV technology employs solar cells and modules those convert the sunlight directly to electricity. Since the sun light is abundant, available free of charge, and cannot be monopolized by a single nation, the future of this technology is very bright. Not surprisingly, the PV technology industry has enjoyed a stupendous yearly growth rate averaging nearly 40 % in the decade 2000-2010. Despite overwhelming acceptance of the PV technology and a forecast of $100 billion business by 2015, the PV energy is costlier than that from the fossil fuel technologies. Thus, it has become essential to identify routes to reduce the cost, which can be achieved through better materials management, development of inexpensive production processes and new techniques to enhance the existing solar cell efficiencies. Using materials in the form of thin films of thicknesses in the range of 1 – 2 μm, it has already been possible to reduce the material consumption. However, the popular second-generation semiconductor thin film solar cells use scarce elements such as indium or tellurium (in Cu(InGa)Se_2/CdTe cells), which limit the further reduction in cost per watt value. A number of binary sulfides are being examined as a possible absorber layers in thin film solar cells grown through cost-competitive techniques. More recently, p-type PbS and n-type CdS thin films have drawn significant interest for their properties suitable for PV applications [2].

The present work concerns with growth of thin films of materials of technological interest using an inexpensive and reliable technique and study of their various properties. The materials chosen for the studies are two binary sulfides, viz. PbS and CdS. The work can be

broadly classified into two parts: Optimized growth and characterization of the films and studies of the p-n heterojunction formed between the layers.

1.1 Thin film solar cells

A Photovoltaic device or a solar cell converts solar light irradiated upon it into electric current. This energy conversion involves two steps: First, the absorption of light produces electron-hole pairs in the devices and in the second step, the generated electron-hole pairs must be separated by the electric field to be collected at electrodes, i.e., the electrons at negative terminal and holes at positive terminal, thus generating electrical power [3]. Accordingly, a functional cell consists of a p-n junction and a pair of electrodes. In practice, however, a couple of window layers are also used. These window layers are n-type semiconductors with wide band gaps so as to allow the sunlight to reach the p-n junction. The absorber layer, the most important layer, is a p-type semiconductor with a high absorption coefficient with a band gap about 1 to 1.5 eV that can match favorably with the solar radiation available on the earth surface. When a junction is formed, electrons from the n-type semiconductor near the interface tend to diffuse into the p-type semiconductor. Similarly, the holes from the p-type semiconductor are diffused into the n-type semiconductor. At the interface, which is called as space charge region or depletion layer, no free carriers are available. The most of solar light is absorbed within the depletion region. The electron-hole pairs generated due to the absorbed photons are rapidly separated by the built-in potential which drifts the electrons and holes apart. In the final step, the electrons and holes must overcome the recombination processes to reach the electrodes and get collected. Thus, in addition to a high absorption coefficient and favorable band gap, a large minority carrier diffusion length and low density of recombination centersare desirable for the absorber layers [3].

1.1.1 Binary sulfide based thin film solar cells

Metal sulfide semiconductors have been traditionally studied for their applications in light emitting diodes, biological labels, photodetectors, etc. because of their unique structural, electrical and optical properties [4-7]. In recent years, their properties such as high absorption coefficient and band gap that can be tuned easily have made them attractive materials as an absorber in solar cell [7]. For example, $CuInS_2$ and Cu_2ZnSnS_4 (CZTS) thin films have become very popular absorber layers and their solar cells have achieved significant efficiencies. On the other hand, a large work function, wide band gap and high transmittance have made n-type sulfide thin films very attractive for use in efficient solar cells. Among the metal sulfide materials, binary metal sulfides are considered to be suitable semiconductors for solar cells for their opto-electrical properties and easy-deposition on larger effective areas at lower cost. Table 1.1 lists the crystal structure, absorption coefficient, band gap and semiconductor type of some metal sulfides. In the followings we describe properties of the two binary metal sulfides, namely PbS and CdS studied in this work.

Table1. 1: Crystal structure, absorption coefficient and semiconductor type of some of the common metal sulfides

Sulfide	Crystal structure	Absorption coefficient (cm^{-1})	Band gap (eV)	Type of semiconductor
PbS	Cubic	10^4 - 10^5	0.37-1.65	p-type [8]
Sb_2S_3	monoclinic, orthorhombic	10^5	1.7-2.47	p-type [9]
CuS	monoclinic, hexagonal	-	1.1-2.0	p-type [10]
SnS	Orthorhombic	10^4 - 10^5	1.01-1.5	p-type [11]
Ag_2S	cubic, monoclinic	10^4	0.9-1.1	n-type [12]
Bi_2S_3	Orthorhombic	10^5	1.3-1.61	n-type [13]
CdS	hexagonal, cubic	10^5	2.4-2.5	n-type [14]
In_2S_3	cubic, tetragonal, trigonal	10^4 - 10^5	1.98-2.81	n-type [15]
ZnS	cubic, hexagonal	10^5 - 10^6	3.6-3.93	n-type [16]

1.2 Literature survey

1.2.1 PbS Thin Films

It is one of the lead chalcogenide (X = S, Se and Te) semiconductors that has been widely used in various applications such as Pb^{2+}-selective ceramic membrane electrodes, decorative coatings, laser technologies, sensors for hydrogen sulfide, humidity sensors, temperature sensors, diode lasers, infrared detectors, etc. [17,18]. PbS constitutes the main reservoir of lead in water-rock interaction in the form of natural mineral galena. It is an abundant, inexpensive p-type semiconductor material that can be potentially used in solar cells without cost-constraints from raw materials [19]. The bulk PbS has a very small band gap of ~ 0.4 eV. However, unlike many other semiconductor, PbS is very sensitive to the grain size of the thin film [18,20,21]. The effective electron and hole masses are relatively small (~8% of the

electron rest mass). Consequently, the exciton Bohr radius of PbS is relatively larger (18-20 nm), which provides a strong confinement regime for electrons and holes, thereby increasing solar radiation absorption in the near-infrared (NIR) region.

PbS crystallizes in the rock salt structure with a lattice parameter of about 5.93Å.**Fig. 1.1** shows a unit cell of PbS in the rock-salt structure. In the typical configuration, each Pb atom is surrounded by 6 S atoms, which are arranged at the corners of an octahedron [22]. Each S atom is also surrounded by six Pb atoms at the corners of an octahedron. A recent study has shown that pressure can induce a phase transition of PbS from cubic to orthorhombic, which is accompanied by a ~3.8% volume collapse [23]. The semiconducting properties are retained in both the cubic and orthorhombic phases; however, they have different electronic transitions: direct and indirect band gaps, respectively.

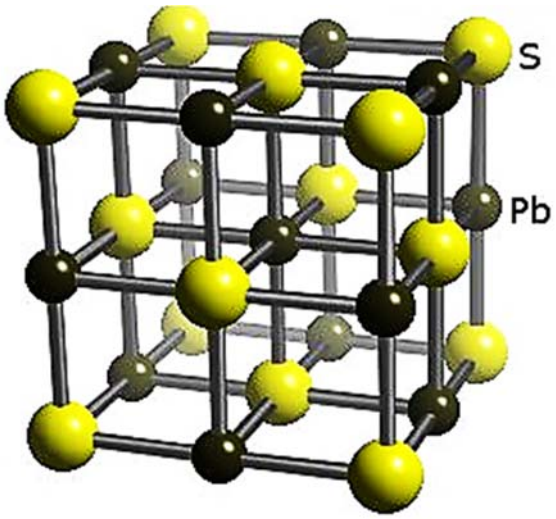

Fig.1. 1: Equilibrium unit cell of PbS [24].

Recently, the effect of multiple exciton generation, i.e., one incident photon was able to create multiple electron-hole pairs, was recently discovered in nanostructures of PbS, which is very promising for solar cell applications [25]. Although the choice of lead sulfide as an

active absorbing layer in a solar cell can be considered unusual as the expected efficiency would be lower than what actually is attained in more conventional CdTe/CdS or $Cu(InGa)(SSe)_2$/CdS solar cells, the recent advancements in tandem solar cells have shown the convenience of developing solar cells based on narrow band gap absorbing materials, such as PbS[26].

1.2.2 CdS Thin Films

CdS belongs to the group II-VI compound semiconductors that have widely studied because of their applications in optoelectronic devices. CdS is an n-type semiconductor with a direct optical band gap, good optical transmittance and tunable resistivity [27]. Bulk CdS can appear in either a zinc blende (cubic) or wurtzite (hexagonal) crystal structure under ambient conditions. The energy (formation) difference between these two structures is very small with the wurtzite structure being slightly more stable. The electrical resistivity of CdS thin films has been reported to be on the order of 10^5-10^7 Ω·cm [28,29]. However, metal doping (gallium-doped CdS) has been shown to reduce the resistivity by up to 10^{-2} Ω·cm and increase the carrier concentration by as much as ~10^{19} cm^{-3}[30]. The optical band gap energy is around 2.4 – 2.5 eV, which mainly depends on film crystal structure, the arrangement and distribution of atoms in the lattice and crystal regularity. It has an absorption coefficient of ~$10^5 cm^{-1}$ at 450 nm. [31].

In photovoltaic applications, CdS has been the best choice as the n-type layer for the CdTe and $CuInGaSe_2$-based solar cells due to its wide band gap, high transmittance and high electrical conductivity [31]. The conduction band position of CdS is much lower than that of other oxide based n-type materials, such as TiO_2 and ZnO, which facilitates electron transport to the n-type layer [32]. More recently, CdS has been used in PbS-based solar cells.

1.2.3 Chemical Bath Deposition (CBD)

There have been many methods to prepare the thin films of metal binary sulfides including those of PbS and CdS. One of the popular methods to deposit PbS and CdS thin films with high degree of reproducibility on large area substrates in an economical way is the chemical bath deposition (CBD) method. In fact, PbS was the first film to be deposited by this method almost a century ago. **Fig. 1.2** shows a typical CBD setup. A substrate, where it is intended to grow the film, is dipped inside the chemical bath set at a temperature for a specified duration. The chemical bath for the deposition consists of precursor, complex agents to dissolve the precursor in solution and chalcogenide source as a reaction source. In the followings, the mechanisms of the CBD process, which depends on the precursors and growth parameters, have been discussed. The case of CdS thin film is taken as an example.

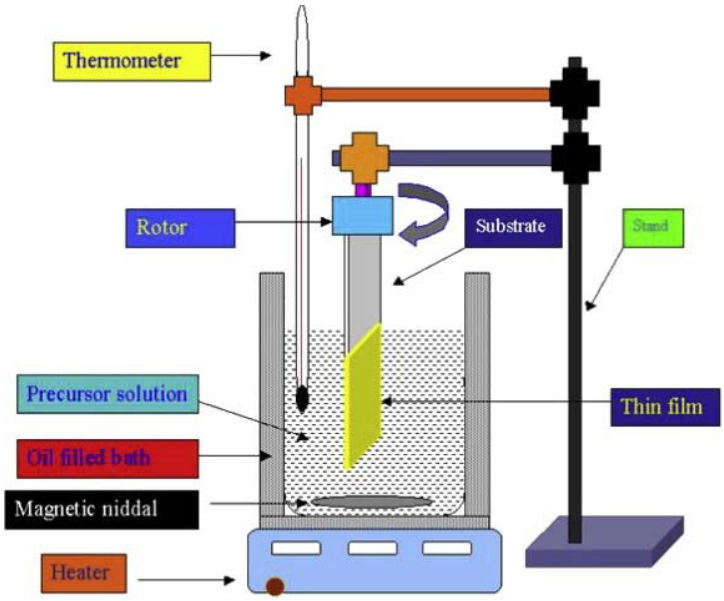

Fig.1. 2: A typical setup for film deposition using the CBD process [33].

1. Ion-by-Ion Mechanism [34]

The simplest mechanism, often assumed to be the operative one in general, is commonly called the ion-by-ion mechanism, since it occurs by sequential ionic reactions. The basis of this mechanism, illustrated for CdS, is given by

$$Cd^{2+} + S^{2-} \rightarrow CdS$$

If the ion product $[Cd^{2+}][S^{2-}]$ exceeds the solubility product, K_{sp}, of CdS, then CdS will form as a solid phase.

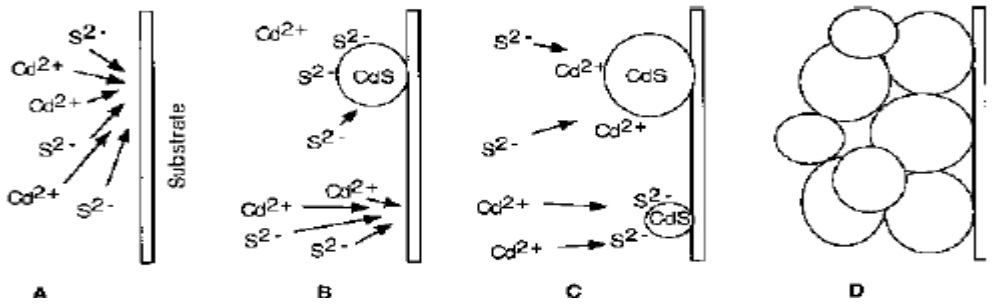

Fig.1. 3: Schematic diagram indicating various steps in the ion-by-ion mechanism. A: Diffusion of ions to the substrate, B: Nucleation of the ions to form the compound nuclei, C: Growth of CdS nuclei by adsorption of Cd and S ions from solution and nucleation of new CdS crystals, D: Continued growth of CdS crystals.

2. Hydroxide Cluster Mechanism [34]

Usually during the CBD process, complexation of the Cd was necessary to prevent $Cd(OH)_2$ precipitation, which would impede the growth of CdS thin films. However, very often $Cd(OH)_2$ (or metal hydroxides in general) are important reaction intermediates in the CBD process. The CdS is then formed by reaction of slowly generated S^{2-} ion with the $Cd(OH)_2$:

$$Cd^{2+} + 2OH^- \rightarrow Cd(OH)_2 \qquad \text{followed by}$$

$$Cd(OH)_2 + S^{2-} \rightarrow CdS + 2OH^-$$

In this case, sulfide formation will occur preferentially at the surface of the hydroxide rather than nucleate separately in the solution. This reaction occurs both at the surface-adsorbed colloids and at those dispersed in the solution. The reaction continues till all of the

hydroxides get conversted into sulfides. Finally, these sulfide particles adhere to each other and grow to fom the continuous sulfide film on the substrate.

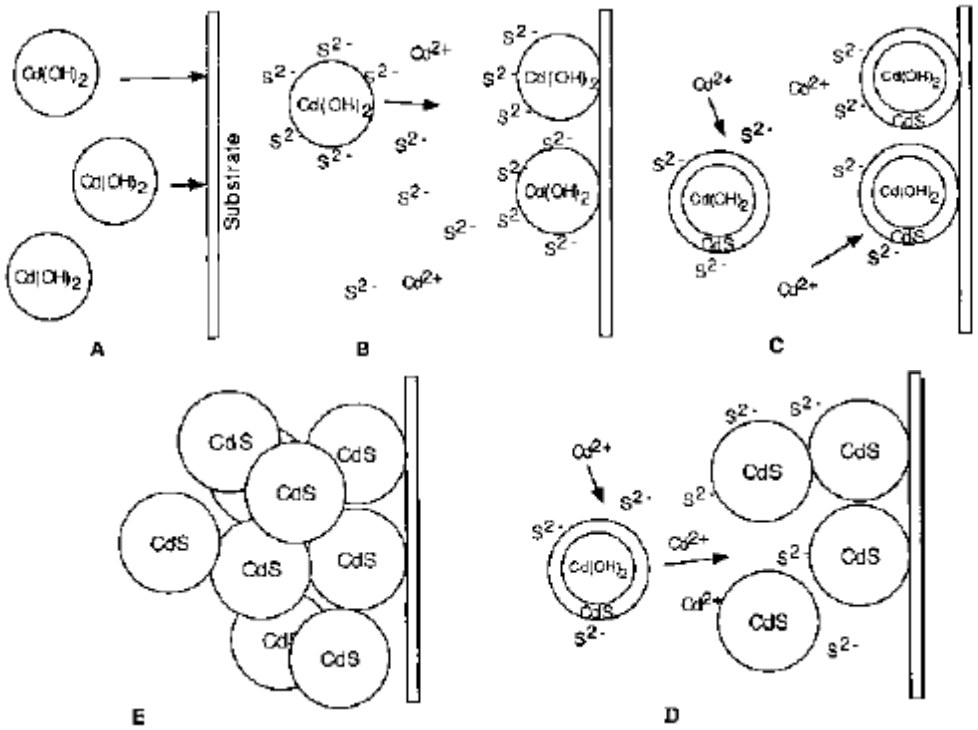

Fig.1. 4:A: Diffusion of hydroxide colloidal particles & adherence to substrate, and (B) react with S ions. This reaction start at the surface of the colloid (on surface and inside solution) and proceeds inward(C). Reaction continues till all hydroxide is converted to sulphide (D); Particles of CdS will adhere to each other to form an aggregated film (E)

3. Complex-Decomposition Mechanism [34]

In many cases, a complex-decomposition mechanism has been proposed. It has been proposed that in the case of strong complexation between the chalcogen compound and the metal ion (e.g., as occurs between thiosulphate and Hg, Ag, and Cu), it is more likely that the weak secondary bond will break easily than the very strong metal - chalcogen bond. Hence, the chemically complex species that contains both metal and sulfur will decompose to form the binary sulfide, as illustrated in **Fig. 1.5**.

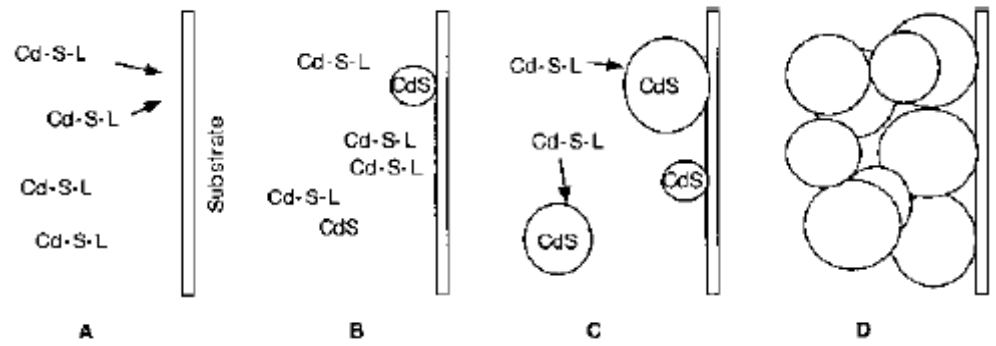

Fig.1. 5: The complex (Cd-S-L, where L is a ligand or part of the S-forming species) decomposes to CdS on the substrate and also homogeneously in the solution (A, B). The CdS nuclei formed grow by adsorption and decomposition of more complex species (C) until a film of aggregated crystals is formed (D) in the same manner as for the previous two mechanisms.

4. Cluster Mechanism [34]

The basis of this mechanism is that a solid phase is formed but, instead of reacting directly with a free anion, it forms an intermediate complex with the "anion forming" reagent. For the example of CdS, this would be given as

$$Cd(OH)_2 + (NH_2)_2CS \rightarrow\!\leftarrow Cd(OH)_2 \,.\, SC(NH_2)_2$$

where $Cd(OH)_2$ is one molecule in the solid-phase cluster. This complex, or a similar one containing also ammine ligands, then decomposes to CdS:

$$Cd(OH)_2 \,.\, SC(NH_2)_2 \rightarrow CdS + CN_2H_2 + 2H_2O$$

i.e., the S-C bond of the thiourea breaks, leaving the S bound to Cd.

1.2.3.1 CBD PbS Thin Films

There have been many studies on growth of PbS thin films by the CBD process. It has been found that the chemical composition of the precursor solution, bath temperature and the pH of the solution are the most important parameters that influence the properties of the resulting films. Accordingly, many researchers have varied these parameters and obtain the desired film properties. In the followings summary of a selected few studies are presented.

Pop et al. have deposited PbS thin films on glass substrates using the CBD process, wherein the bath contained lead nitrate, thiourea, sodium hydroxide and hydroxylamine [35]. They varied the deposition time to prepare films of different thicknesses in the range of 120 to 540 nm, which showed varied degrees of photosensitivity. Patil et al. deposited PbS thin films on glass substrates from the solution containing 0.1M lead nitrate, 0.1M thiourea. They maintained the pH at 9 and a deposition temperature of 300 K. Despite a longer deposition time of 2 to 7 hours, the films had very small crystallites of dimensions of a few nanometers. The films exhibited p-type conductivity of order of $10^{-4}(\Omega cm)^{-1}$[36].In a similar study, Seghaier et al. used the reagents as 0.175M lead nitrate, 0.1M thiourea and sodium hydroxide at 298 K. However, they prepared the films for small deposition time of 10-90 min. [37]. In 2007 Osherov et al. deposited PbS thin films using the precursor solutions of lead nitrate of 0.01- 0.175 M, thiourea of 0.057 – 1 M and sodium hydroxide of (0.146-0.57)M at 313 K. The deposition time of the film was varied in the range of 20-60 min. They found that the deposition temperature and time had a major role in obtaining nanocrystalline films. The domain size increased with film thickness and it resulted in a single crystal film with less or fewer defects [38].Jana et al. fabricated PbS thin films on glass substrates. Reagents used for the film were 0.0498M lead nitrate, 0.02M sodium hydroxide and 0.118M thiourea. The deposition temperature of the bath was ~ 303 K. The deposition time of the bath was for 1 hour of duration. They found that the band gap value of the resulting films is much higher than the bulk value (0.41 eV) due to quantum confinement of the carriers in the nanocrystallites [39]**.** Raniero et al. deposited PbS thin film by using a solution of lead nitrate, sodium hydroxide and thiourea. Thirty minutes after immersing the substrates in the solution, the thickness of the film remained unchanged, suggesting that Pb and S ions had been fully consumed. Thus, thicker films were obtained depositing additional PbS from a fresh solution. Photoconductivity measurements showed that the heat treatment activated the mechanism of

photoconduction [40]. In 2011, Abbas et al. deposited PbS nanocrystalline thin films on glass substrate using Lead acetate and thiourea as a sources of Pb and S, and triethanolamine as a complexing agent. The films were deposited at different solution temperature and at various deposition times. They found that band decreased marginally from 2.31 to 2.19 eV with increasing film thickness [41]. More recently, Obaid et al. have synthesized nanocrystalline PbS thin films on glass substrates from solutions composed of 0.1M lead nitrate and 0.1M thiourea dissolved in distilled water. Deposition time was varied ranging from 30 to 120 minutes. Atomic force microscopy (AFM) images confirmed narrow particle size distribution, and increase in surface roughness with the increase in deposition time [42].

Tohidi et al. (2012) synthesized high quality PbS thin films on glass substrate from two baths with different compositions. One of them (bath-I) contained an aqueous solution of lead acetate, thiourea, sodium hydroxide, and the second (bath-II) had additional triethanolamine. The introduction of triethanolamine reduced the grain size and increased the optical band gap of the PbS nanoparticles [43]. Altiokka et al. in 2013 deposited PbS thin films using a bath containing 0.0089M lead nitrate, 0.1460M sodium hydroxide, 0.510M thiourea and 0.00023M sodium sulfate. The temperature of the bath was maintained at 303K. It was found that the rate of precipitation, which depends on the precursor concentration, affects the formation of pinhole [44]. Preetha et al. have studied the effect of lead sources on the film properties. They grew films using four different lead sources, namely lead nitrate, lead acetate, lead chloride and lead sulphate in alkaline medium along with thiourea as sulphur source. The average crystallite sizes are found to be in the range 13-24 nm. The direct band gap energy values were in the range of 1.86 -2.61 eV. The electrical conductivity varied in the range 33.6-7.62 $\times$ $10^{-9}(\Omega\ cm)^{-1}$ [45].Valenzuela et al. synthesized nanocrystalline and photosensitive PbS thin films from reaction solution composed of 31mM lead acetate,

125mM sodium hydroxide, 75mM thiourea, 25mM triethanolamine and 5% ethylic alcohol. Thin film deposited for a reaction time of 4 h had a thickness of ~181 nm, crystallite size of ~14 nm, an energy band gap of ~0.93 eV and light conductivity of 0.307 $(\Omega cm)^{-1}$[46]. Gode et al. deposited PbS thin film by varying the deposition time at room temperature. The precursor solutions for the deposition of the films involved 5ml 0.5M lead acetate, 5ml 2M sodium hydroxide, 6ml 1M thiourea and 4ml 0.5M tri-sodium citrate. The time varied from 100 min to 145 min and by studying the optical properties, they found that the optical band gap decreased from 2.65 to 2.50 eV with increasing deposition time. The electrical conductivity of the PbS film increased from 1.791×10^{-6} to 1.655×10^{-3} $(\Omega\ cm)^{-1}$ with increasing deposition time [47].

1.2.3.2 CBD CdS Thin Films

Similar to the case of PbS thin films by the CBD process, the sources for Cd and S, concentration of the precursor solution, bath temperature and the pH of the solution critically affect properties of the films. Many researchers have prepared the films from solutions containing ammonia based compounds, which are toxic and environmentally dangerous when used in large scale. Consequently, there are growing efforts to synthesize these films using ammonia free bath solutions.

Herrero et al. fabricated a CdS thin film on fluorine doped tin oxide (FTO) coated substrates. The precursor solution was made from 0.025M cadmium chloride, 0.035M thiourea and 1.7M ammonium. The temperature of the bath was maintained at 333K, and the reaction was allowed to continue at a pH 12[48]. Vigil et al. deposited the CdS thin films on glass substrates using precursor solutions made from 0.02M cadmium chloride, 0.5M potassium hydroxide, 1.5M ammonium nitrate and 0.2M thiourea at a bath temperature of 353K. They

found that post-deposition annealing influenced the crystalline quality, lattice parameter, the grain size and the optical absorption [49]. H. Metin et al. deposited CdS thin films on a glass substrate at 333 Kusing a different Cd source, i.e.,cadmium sulfate. They usedan alkaline solution of 1M cadmium sulfate, 1.4M thiourea, 2.25M hydrazine and 25% ammonium. The films contained both cubic and hexagonal structures. The percentage of hexagonal structured crystallites in the films was increased after annealing [50]. Soundeswaran et al. deposited the films using similar compounds, i.e., 0.01M cadmium sulfate, 0.1M thiourea, 0.1-0.325% ammonium sulfate and ammonium. The as- deposited films were cubic and after the annealing, the crystallinity improved accompanied by a structural change from cubic to hexagonal phase [51].

Prabahar et al. found out the effect of the pH value on the CdS thin films. They used a precursor solution made from 1M cadmium chloride, 1M thiourea, $C_6H_{15}N$ (1-butanamine) and ammonium. The films were prepared on glass substrates at 333-363 K for 30-60 minutes and the pH was varied from 9 to 11. It was observed that the films prepared with the pH value of 10 have better structural and optical properties [52]. Quiebras et al. deposited CdS thin films on FTO coated substrates at 348K deposition temperature for 15-180 min. and the film thickness was 100-280 nm. They made the chemical solution by adding 0.12M cadmium chloride, 2M ammonium and 0.3M thiourea. They found out that the growth rate is faster when the quantity of thiourea is much greater than the cadmium chloride concentration in the solution. Furthermore, when the S/Cd ratio was higher, the band gap increased [53].Montijo et al. have also prepared CdS thin films using chloride Cd source. The precursor solution was composed of 0.05M cadmium chloride, 0.5M sodium citrate, 0.5M potassium hydroxide and 0.5M thiourea [54]. Archbold et al. deposited CdS thin film on glass substrates at 303K for

75 min with solution pH of 12. The precursor solution was made by using 0.001M cadmium chloride, 0.012M ethylenediamine, 0.01M sodium hydroxide and 0.01M thiourea [55].

Khallaf et al. deposited the films using different Cd sources and studied the film properties. The Cd sources were cadmium sulfate ($CdSO_4$), cadmium chloride ($CdCl_2$), cadmium iodide (CdI_2), and cadmium acetate ($Cd(CH_3COO)_2$). Film growth rate, stoichiometry and band gap were found to be sensitive to the Cd source used. Film thickness was found to decrease in the order $CdSO_4$, $Cd(CH_3COO)_2$, $CdCl_2$, CdI_2. However, the band gap was found to decrease in the order $CdSO_4$, $Cd(CH_3COO)_2$/CdI_2, $CdCl_2$.For the cadmium chloride and cadmium iodide solutions, the films were highly stoichiometric. The lowest resistivity and highest mobility and band gap obtained were in the case of cadmium sulfate. All films were found to be cubic, regardless of the Cd salt used [56].

1.2.4 PbS- CdS heterojunctions

Although PbS and CdS thin films have long been studied, their extensive use in photovoltaics has gained popularity recently. After the observation of extreme tunability of band gap in the PbS quantum dots, PbS is being studied with renewed interest as an absorber material in solar cells. Many researchers have reported about PbS solar cells with different structures or combinations to obtain effective photovoltaic cells and the focus of such studies is based on the PbS quantum dots [57-62][63-68]. However, there are a few disadvantages associated with PbS quantum dots that include difficulties in (i) controlled growth of monodispersed quantum dots, (ii) stability in air, and (iii) long term stability of the resulting devices.

On the other hand, easy synthesis of the PbS thin films offers possibilities to prepare heterojunction and fabricate photovoltaic devices. Table 1.2 shows selected examples of PbS

absorber thin films used in solar cells. The table also includes the heterojunction sulfide materials and the key performance parameters.

Table1. 2: Performance of selected PbS based thin film solar cells

Process for PbS film	Solar cell structure	J_{sc} (mA/cm^2)	V_{oc} (V)	FF (%)	η (%)	Year (Ref)
CBD	FTO/Bi_2S_3/PbS/C/Ag	6	0.28	36	0.5	2011 [69]
CBD	ITO/CdS/PbS/C	14	0.29	36	1.63	2011 [70]
(MA) CBD	ITO/CdS/PbS/Al	8.8	0.28	23	1.68	2013[71]
CBD	FTO/CdS/Sb_2S_3/PbS/Ag	1.28	0.63	29	0.24	2008 [72]

With the n-type layer Bi_2S_3, solar cells with the structure FTO/Bi_2S_3/PbS/C/Ag has been reported that had an efficiency of about 0.5%. It was thought that the narrow band gap of Bi_2S_3may have limitations in boosting the cell performance. More recently, the CdS/PbS heterojunctions have been investigated. The initial study of the photoelectric effects of CdS/PbS stacks was reported in 1972 and triggered further studies to improve and optimize CdS/PbS junctions [73]. The CdS layer is considered as a suitable choice because of its wide band gap of 2.4-2.6 eV, high transmittance and high electrical conductivity [74]. Moreover the conduction band position of CdS is much lower than that of other n-type possible candidates such as TiO_2 and ZnO, which facilitates electron transport to the n-type layer [73]. Ramirez-Bon et al. fabricated solar cells with the structure of glass/ITO/CdS/PbS/conductive graphite. Fig. 1.6 shows the schematic diagram of the cross-section of the device. They used n-type CBD CdS (130 nm) and p-type CBD PbS (4200 nm) at ~70 °C. They obtained an efficiency of 1.63 % [61]. Soon after, Obaid et al. fabricated solar cells with the structure: glass/ITO/CdS(340 nm) /PbS (1400 nm)/Al. Both CdS and PbS were grown by the

microwave assisted CBD process. They obtained the efficiency of ~1.35 % and fill factor (FF) of 0.546[75].Recently the same group has improved the efficiency to ~1.68%. Saikia et al. fabricated a solar cell using microwave assisted chemical bath deposition technique. The surface morphology shows that the thin films were nanostructured, homogeneous, without any pinholes or cracks and covered the substrate well. The efficiency of the cell found to be 1.668%[76].Messina et al. reported that using $Sb_2(S,Se)_3$ interlayers between CdS/PbS may enhance charge transfer through the junction and, thus, cell efficiency[77].

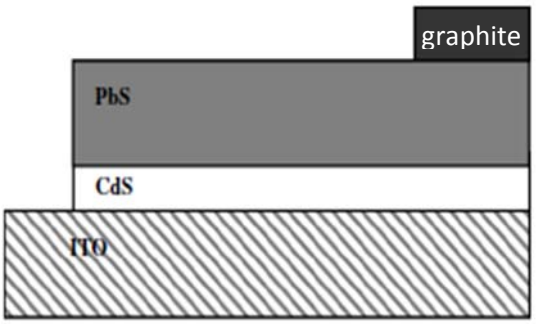

Fig.1. 6: Schematic diagram of cross-section of the device used byRamirez-Bon et al. [70].

1.3 Motivation and Objectives

The discussions in the preceding sections indicated that the use of PbS/CdS heterojunctions for photovoltaics is in the nascent stage and the photovoltaic performance is less than 2 %. Since it has been easier to grow the PbS and CdS thin films with high degree of reliability and reproducibility, it can be expected that the properties of both the films can be tailored suitably to improve the performance. Hence, there is a large scope to enhance the efficiency of PbS/CdS heterojunction based solar cells. This has been the primary motivation of the present work. Secondly, these films have been often prepared in ammonia solutions, which is toxic and environmentally dangerous. We intend to fabricate the films in an ammonia-free CBD process.

The key objectives of the present wok can be outlines as followings:

- Fabrication of PbS and CdS layers using the CBD process which has the advantage of being simple, inexpensive and suitable for large area deposition.
- Structural, optical and electrical characterization of thin films using various techniques.
- Investigation of various process parameter dependence of film properties and identification of sets of process parameters concurrent to optimum quality of films for photovoltaic applications
- Fabrication of PbS/CdS heterojunctions and study its properties.

This thesis is organized in the following way. Chapter 1 gives brief introduction to the materials chosen, motivation and objective of the present work. Chapter 2 presents the experimental techniques used in this work. It also includes the details of the film growth procedures, chemicals used, etc. Chapter 3 describes the results and discussions on the PbS and CdS thin films. In Chapter 4, results of studies on PbS/CdS heterojunctions have been presented. The conclusions and the future scope of this work have been presented Chapter 5. The references have been provided at the end.

CHAPTER 2

EXPERIMENTAL TECHNIQUES

In this chapter, an account of the experimental techniques used for the growth and detailed characterization of the PbS and CdS thin films is presented. Section 2.1 gives a brief description of the film preparation. Details of the various techniques used for characterization of the films are presented in section 2.2.

2.1 Growth of PbS and CdS thin films

There have been a variety of methods reported in literature to prepare the binary sulfide thin films that includes vacuum techniques such as spray pyrolysis (SP), chemical vapor deposition (CVD), thermal evaporation (TE) and sputtering, etc. and many solution processes [78-81]. Amongst all, the CBD process has emerged as the most attractive method due to easy control of process parameters, ability to prepare films at low temperatures, and large area deposition [82].In this work, individual PbS and CdS layers, and CdS/PbS bilayers (heterojunctions) were prepared by the CBD process. Typical growth mechanisms in the CBD processes have been presented detail in section 1.2.3. In this section, the reagents and the specific experimental conditions for growth of the films are described.

In this work, lead acetate ($Pb(CH3COO)_2.3H_2O$) and thiourea were used as sources for Pb and S in the CBD process. Stock solutions of 2.5 ml of 0.5 M $Pb(CH_3C00)_2.3H_2O$, 3 ml of 1 M thiourea, 2.5 ml of 2 M NaOH and 2 ml of 1M triethanolamine were prepared in distilled water. **Fig. 2.1** shows the photographs of the prepared stock solutions. The total volume of the deposition bath was made 100 cm^3. The reagents were added under constant stirring. The glass slides were first washed with detergent solution, followed by ultrasonic cleaning in DI

and acetone for 10 min each. The cleaned glass slides were kept vertically in the solution. In typical conditions, only one substrate was used to prepare the film on an area of 2.5 cm × 2.5 cm. The substrates were introduced after 15 minutes of preparation of the bath solution. Stirring of the solution was maintained at about 800 RPM for the entire duration of deposition (starting from addition of reagents till removal of substrates from solution). All films were deposited in a single step. It was noted that the color of the solution slowly changed to black with deposition time. The rate at which the color changed was dependent on the bath temperature. **Fig. 2.2** shows photographs of such a change. The deposition time was varied from 10 to 180 mins. To study the effects of bath temperature on properties of the films, the bath temperature was varied from 40 to 80 °C. For measuring the temperature, a thermometer (with an accuracy of ± 2 °C) was kept inside the solution for the entire period of deposition. After the specified time, the substrates with the coating were removed from the solution and were rinsed in DI water followed by air-drying.

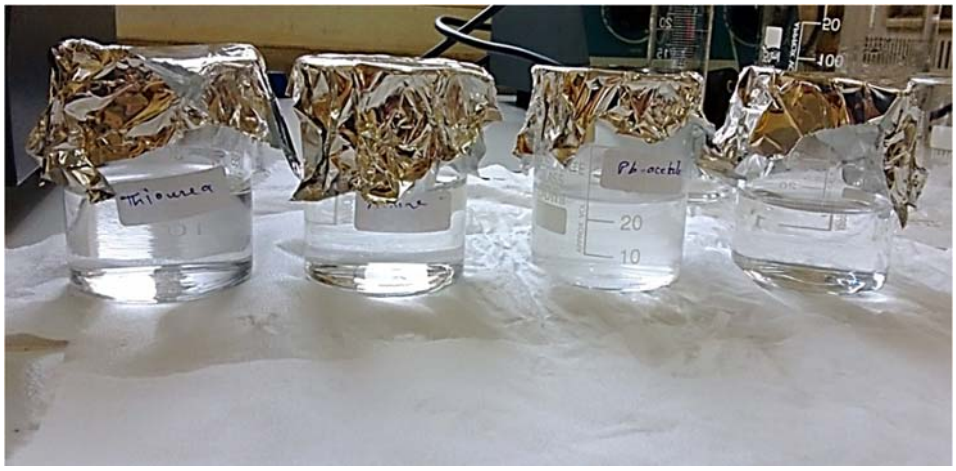

Fig.2. 1: Photographs of the stock solutions of thiourea, triethanolamine, lead acetate and NaOH.

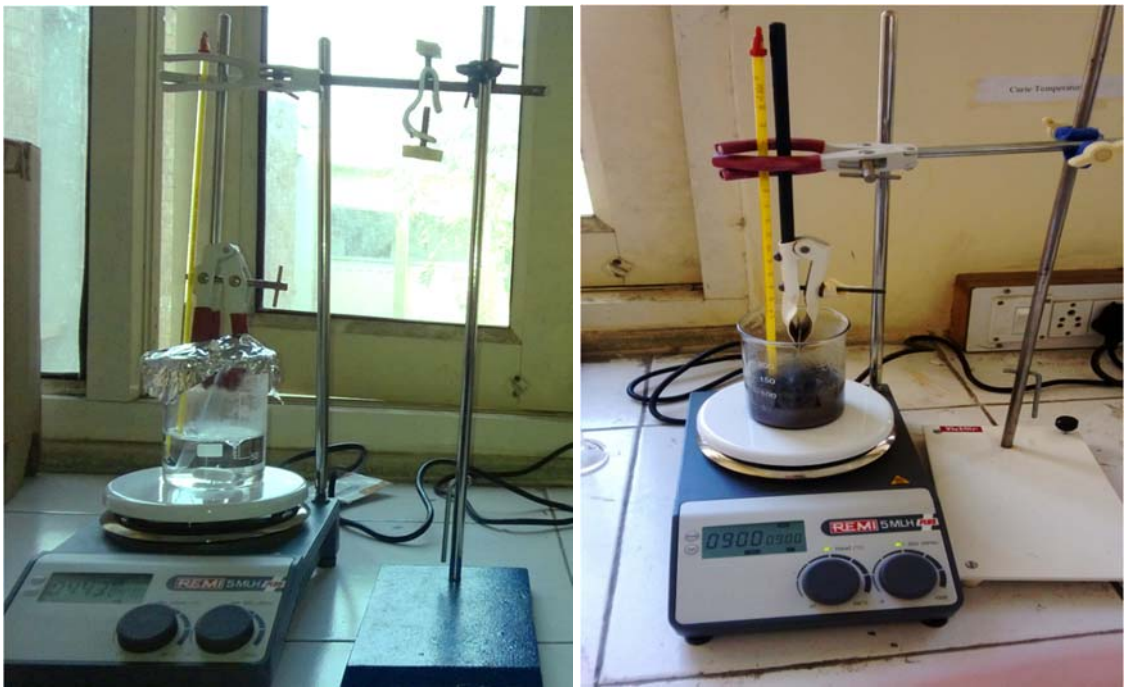

(a) (b)

Fig.2. 2: The color of the bath solution changes with time. The photograph in (b) was taken after 30 min from starting of the deposition.

Similar to the steps followed for the deposition of the PbS films, CdS thin films were grown by the CBD process using cadmium chloride ($CdCl_2$) and thiourea as sources for Cd and S, respectively. The deposition of CdS films was done in a reactive solution prepared by sequential addition of 25 ml of 0.5 M cadmium chloride, 20 ml of 1 M sodium citrate, 5 ml of 1M of KOH, 20 ml of buffer NaOH solution having pH= 10 and 10 ml of 1 M thiourea in a 100 ml beaker. The reagents were added under constant stirring. In a single deposition process, only one cleaned glass slide was introduced vertically in the solution after 15 minutes of preparation of the bath solution. In typical conditions, film was deposited on an area of 2.5 cm × 2.5 cm. The deposition time was varied from 10 to 180 mins and the bath temperature was varied from 40to 80 °C. After deposition, the samples were rinsed in DI water followed by air-drying.

2.2 Characterization techniques

2.2.1 Structural characterization using X-Ray diffraction (XRD)

Analysis of the XRD patterns allows the determination of phase purity, structure, crystallite size and strain, if any, of the crystalline materials [83]. The technique employs X-rays, which are electromagnetic waves with wavelengths of order of a few angstroms. When a parallel beam of X-rays is made to strike a crystalline material, they are of scattered at different angles owing to the periodic nature of atomic arrangement in the crystalline material. Thus, one gets a diffraction pattern characterized by peaks of substantial intensity at specific angles. **Fig. 2.3** shows the principle of X-ray scattering by rows of atoms. The lattice spacing (d_{hkl}) can be calculated using the well-known Bragg's relation,

$$2d_{hkl} \sin\theta = n\lambda \qquad \ldots\ldots\ldots\ldots \qquad (2.1)$$

Where, 2θ is the corresponding Bragg angle, n is the order of diffraction (usually the 1st order ones are considered), and λ is the wavelength of the X-rays employed in the measurement.

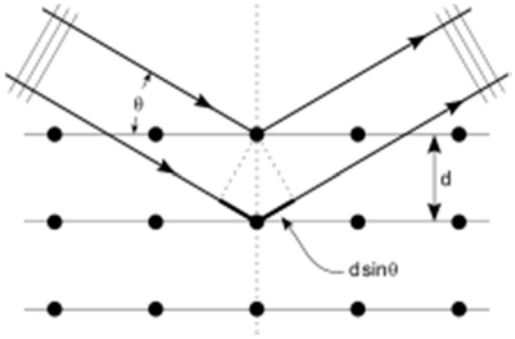

Fig.2. 3: Diffraction of X-ray by planes of atoms

In the present work, the measurements were carried out in a PAN analytical (model: X'Pert PRO) XRD unit using Cu-Kα radiation in the conventional θ-2θ mode. By comparing with the established JCPDS data, the phases of the films were identified and the peaks in the patterns were indexed.

2.2.2 Surface microstructure studies

Surface microstructure of the films and its dependence on the process parameters were studied using scanning electron microscopy (SEM) and atomic force microscopy (AFM). There are many excellent books which deal the SEM and AFM in detail [84-88]. In the following sections a brief account of each technique is given.

2.2.2.1 SEM

SEM allows imaging of surfaces using electrons similar to an optical microscope that uses visible light. The advantages of SEM include greater magnification and much greater depth of field. In the SEM, a fine focused beam of electrons with energies upto 30-40 keV is raster-scanned across the sample surface, which generates secondary electrons, backscattered electrons, and characteristic X-rays. Typically, the secondary electrons produced due to the inelastic interactions between the incident electron beam and the electrons in the sample are collected to form an image of the surface. Elastic interaction between the incident electrons and the sample electrons generates backscattered electrons. Imaging with backscattered electrons gives contrast based on atomic number to resolve composition variations, as well. However, the surface features are not resolved properly since backscattered electrons can escape from deep within the sample due to their high energy. The emitted X-rays are analyzed to obtain qualitative and quantitative chemical information.

The SEM measurements were carried out on the PbS and CdS films using JEOL (model: JSM-6510) scanning electron microscopes. Some of the samples were also investigated using and JEOL (model: JSM-6010LV) scanning electron microscope. Apart from plane-view images, cross-sectional views of selected samples were also obtained. The operating voltage used during the measurements was in the range of 10 to 20 KV.

2.2.2.2 AFM

AFM is one of the surface scanning probes that provide 3-dimensional information in real space with sub-nanometer spatial resolution. AFM has several advantages over other surface imaging techniques. It allows imaging of insulating samples without any special treatment like metal coatings, required in SEM. Besides, AFM measurements can be carried out in ambient air or even in liquid environment. The working principle of AFM is based on sensing the forces between a probing sharp tip and the sample. The tip is held at the end of a cantilever which provides a restoring force to counter that arising from the tip-sample interaction, such as van der Waals, capillary, electrostatic etc. Change in the deflection of the cantilever is, thus, a measure of the changes in the tip-sample forces. The images are taken by scanning the sample relative to the probing tip and measuring the deflection of the cantilever as a function of lateral position. A beam-deflection method is usually used to detect the deflection of the cantilever. A light beam is reflected from the rear side of the cantilever and is monitored by a position sensing photo-detector.

There are mainly two modes of operation of AFM, namely, static and dynamic modes. In the 'static mode' of operation, the tip deflection is used as a feedback signal. When the tip is very close to the surface, the attractive forces can be very strong which can cause the tip to snap in to the surface. Therefore, 'static mode' imaging is usually done in contact where the overall force is repulsive. In this mode, commonly known as 'contact mode', the force between the tip and the surface is kept constant during scanning by maintaining a constant deflection. In the 'dynamic mode', the cantilever is externally oscillated at frequencies very close to its resonance frequency. The changes in amplitude, phase and resonance frequency due to the tip-sample interaction forces are monitored to gain information about the sample surface. The 'dynamic mode' of operation can be of 'non-contact mode' or 'tapping mode'. In the 'non-

contact mode' the tip is very close to the sample surface, thus in the attractive force regime. When operated in the tapping mode, the oscillating cantilever is positioned above the sample surface such that it only taps the surface for a small fraction of time. This is similar to 'static mode' operation, but for a very short time which results in a large decrease in the lateral forces.

The AFM measurements for selected samples were carried out in contact mode in air using SOLVER Next - NT – MDT. The images were acquired at various locations and at different magnifications.

2.2.3 Optical transmittance and band gap measurement

The properties of a thin film that determine its suitability for photovoltaic applications are optical transmittance, absorbance and band gap. UV-visible-NIR spectroscopy is used for evaluation of these properties and the measurements are done using a UV-visible-NIR spectrophotometer. The basic principle of the UV-visible-NIR spectroscopy is based on the fact that as light passes through a material, its intensity decreases exponentially. This is expressed through the Beer-Lambert law:

$$I = I_0 e^{-\alpha d} \qquad \ldots\ldots\ldots\ldots \quad (2.2)$$

Where,I_0 is the intensity of the light incident on the sample, α is the absorption coefficient and d is the thickness of the sample. Rearrangement of Eq. (2.2) yields

$$\alpha = -\frac{1}{d}\ln\left(\frac{I}{I_0}\right) \qquad \ldots\ldots\ldots\ldots \quad (2.3)$$

Often the ratio I/I_0 is just the transmittance (T) of the sample. Hence, the absorption coefficient (α) and the transmittance (T) of the film are interrelated through the equation

$$\alpha = -\frac{1}{d}\ln T \qquad \ldots\ldots\ldots\ldots \quad (2.4)$$

If the wavelength (or photon energy) dependence of α is known, one can estimate the fundamental absorption edge (band gap) by plotting $(\alpha h\nu)^2$ as a function of hν, following the relation for the direct allowed transition,

$$\alpha = A_1/h\nu\ (h\nu - E_g)^{1/2} \qquad \ldots\ldots\ldots\ldots \qquad (2.5)$$

Where, A_1 is a constant and E_g is the energy gap. In the plot of $(\alpha h\nu)^2$ vs hν, the extrapolated intercept on the abscissa gives the value of E_g. This procedure has been previously used for determining the band gaps of semiconducting thin films including PbS and CdS [89].

The key components of a spectrophotometer include a light source, a sample holder, a monochromator and a detector. The detector is typically a photomultiplier tube, a photodiode, a photodiode array or a charge-coupled device (CCD). Single photodiode detectors and photomultiplier tubes are used with scanning monochromators, which filter the light so that only light of a single wavelength reaches the detector at one time. Fixed monochromators are used with CCDs and photodiode arrays. As both of these devices consist of many detectors grouped into one or two dimensional arrays, they are able to collect light of different wavelengths on different pixels or groups of pixels simultaneously.

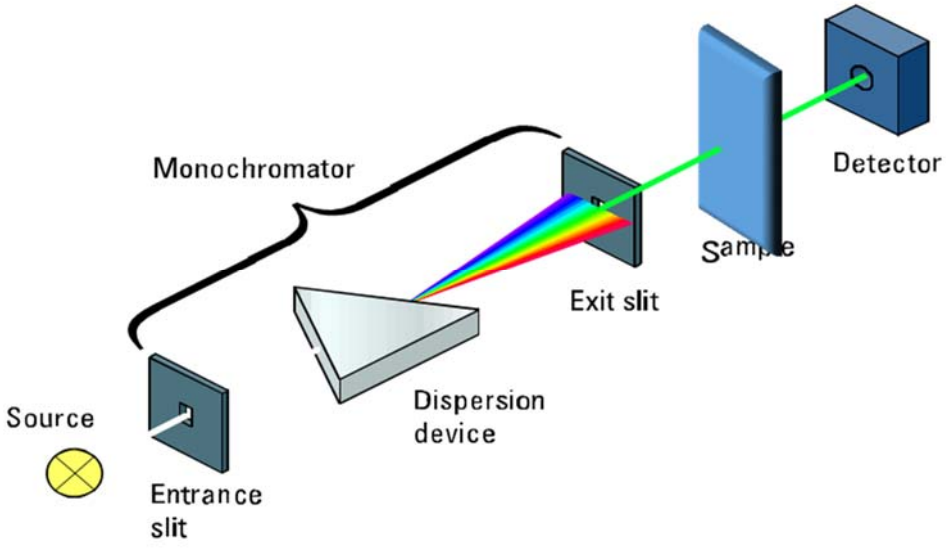

Fig.2. 4: Single beam UV- visible spectrophotometer [90]

In a double-beam instrument, the light is split into two beams before it reaches the sample. One beam is used as the reference; the other beam passes through the sample. The reference beam intensity is taken as 100 % transmission (or 0 %absorbance), and the measurement displayed is the ratio of the two beam intensities.

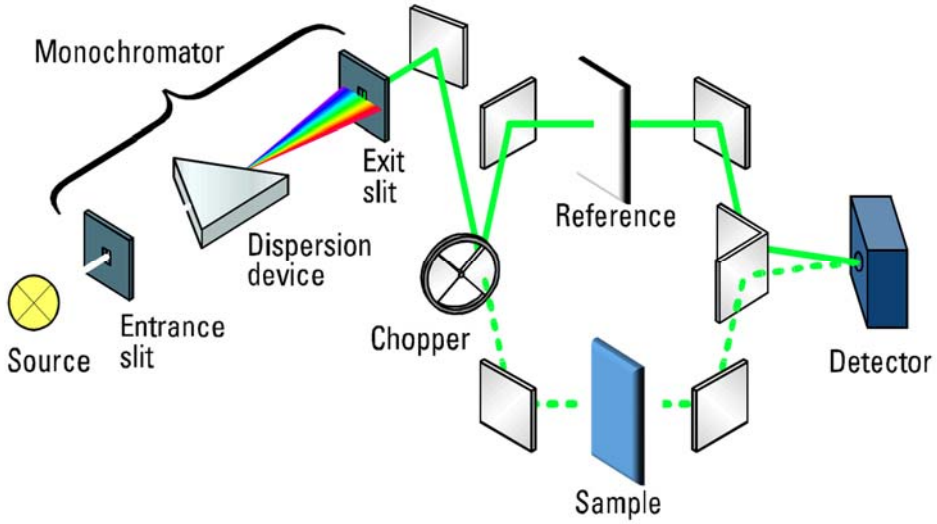

Fig.2. 5: Double beam UV- visible spectrophotometer [90]

Optical transmittance of the PbS and CdS thin films as a function of wavelength in the near-IR and visible regions was measured using a SHIMADZU UV-VIS spectrophotometer (model: UV-2600/2700). Using the procedure described above the optical band gap of the films was determined.

2.2.4 Electrical Measurements

Current density-voltage (J-V) measurements were obtained using an I-V curve analyzer (IviumStat, Ivium Technology) and a solar simulator (Sun 2000, ABET technology) under AM 1.5. For the J-V measurements (dark and light responses), films were grown on cleaned indium tin oxide (ITO)-coated glass substrates. The ITO coating was used as one of the electrodes. For the other electrode, Al was evaporated through a mask (of area 3 mm × 3

mm.The thickness of the Al layer was about 120 nm. In some cases, 1 nm thick LiF was deposited by thermal evaporation before deposition of Al. Both LiF and Al were deposited at a pressure level better than 2×10^{-6} torr. J – V measurements were carried out on the following structures: (i) Glass/ITO/ PbS/ LiF/ Al, (ii) Glass/ITO/PbS/Al, (iii) Glass/ITO/ CdS/ PbS/LiF/Al and (iv) Glass/ ITO/ CdS/ PbS/ Al. The intention of such structures was to evaluate the performance of Schottky junction between the PbS with metals while that of the last two ones was to assess the photovoltaic performances. The light was made incident from the substrate side. **Fig. 2.6** summarizes the configuration of the samples used in this work.

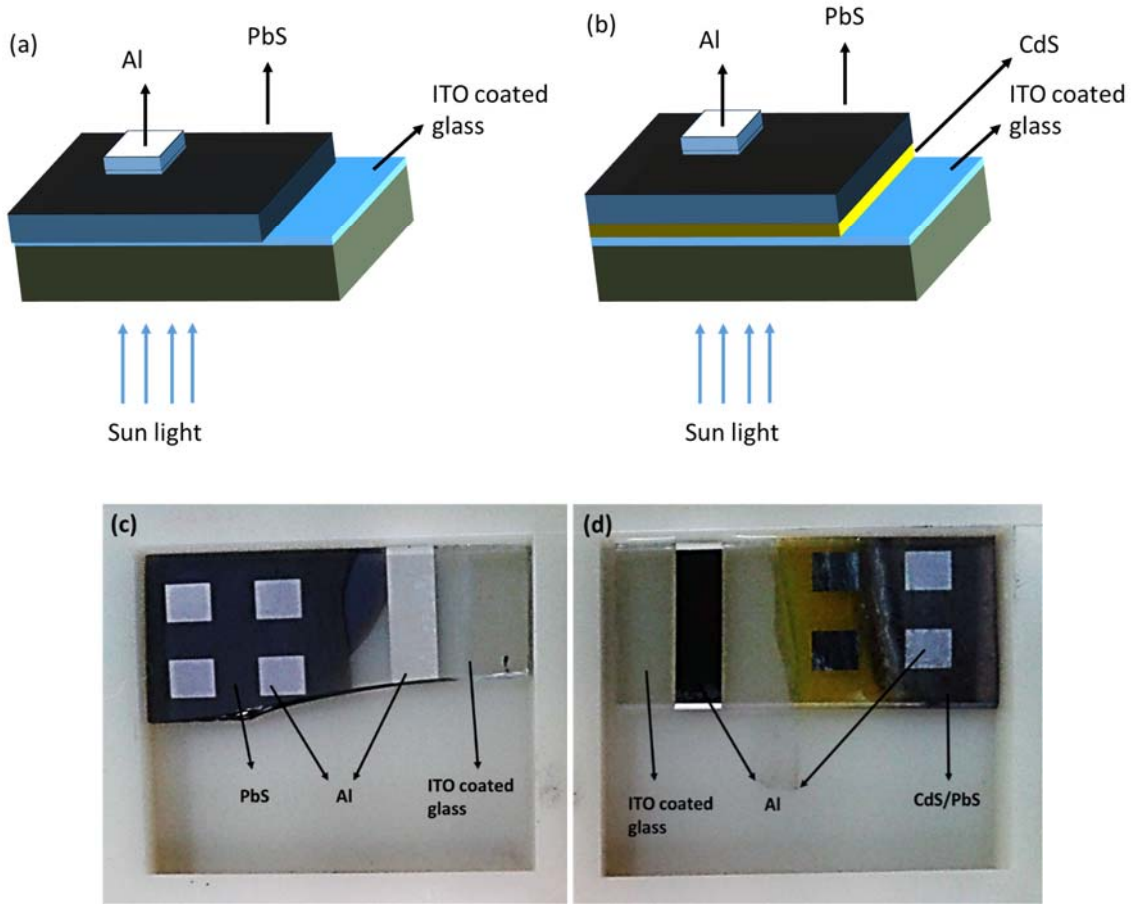

Fig.2. 6: Multilayer structures used for J-V measurements. Measurements were done in dark conditions and with light at 1.5 AM conditions. In a separate set of samples a 1 nm thick LiF layer was used between PbS and Al layers. The configuration (a) was used to study the property of the Schottky junction between PbS and Al. The top-view photographs of the corresponding samples are shown in (c) and (d).

CHAPTER 3

CHARACTERIZATION OF PbS AND CdS THIN FILMS

This chapter deals with the detailed characterization of the PbS and CdS thin films grown by the CBD process as outlined in the previous chapter. The chapter is broadly dived into two sections separately concerning with PbS and CdS films. The effects of deposition time followed by the role of bath temperature on the film properties have been presented.

3.1 Evolution of properties of PbS thin films with time

Suitable thickness of the films is an important parameter for optimum performance in any device. For instance, about 200 nm has been considered as the optimum thickness in the PbS-based thin film solar cells [91]. A thickness below 200 nm results in very poor absorption of incident photons responsible for the creation of the electron-hole pairs, while that above 200 nm results in higher recombination because the diffusion length of the minority carriers in PbS is only about 200 nm. However, controlling the thickness of the films in the CBD process is more complicated than that in the physical vapor deposition processes such as sputtering or evaporation. In the case of sputtering or evaporation, there is a constant source of the depositing species and hence, thickness often exhibits linear dependence on deposition time. However, in the CBD process, the ions get depleted with deposition time. Thus, for a given starting concentration of the bath solution, the deposition rate saturates with deposition time, and multiple deposition steps (i.e., putting the coated substrate in a freshly prepared bath subsequently) have been required to attain the desired thickness [2]. In this work, it was attempted to prepare the films at low bath temperature for different deposition times and examine their properties, and hence determine the growth time most suitable for possible device applications.

Since from the industry point of view, fabrication of the devices at low temperatures is desirable for minimizing the thermal cost, it was intended to prepare the films at room temperature. It was found that no film could be deposited at ~30 °C, in spite of a very long deposition time. When the bath temperature was increased to about 40 °C, films could be successfully deposited, however. The evolution of film properties with deposition time was investigated using XRD, SEM, AFM, UV-visible spectroscopy.

3.1.1 Results of the XRD measurements

Figure 3.1 shows typical XRD patterns of the PbS thin films grown on glass substrates at 40 °C for different deposition times. The pattern obtained for a deposition time of 30 min shows only a broad hump in the range of 20° to 35° corresponding to the amorphous glass substrate. The absence of any peak indicates that the deposited species have not been crystallized. The film, if any, might have been composed of very small crystallites. In fact, the SEM results presented in the following section shows deposition of a very thin discontinuous film comprised of particulates of nanometer scale. However, as the deposition time was increased, a clear evolution of peaks at was observed. All films of higher deposition time (> 30 min) were characterized by five Bragg peaks, namely at about 26.02°, 30.09°, 43.03°, 50.97° and 53.36°. The peaks were identified with the planes (111), (200), (220), (311), and (220), respectively corresponding to the cubic PbS phase, consistent with the reference data [JCPDS 05-0592]. It was observed that the peak positions and the peak intensity remained approximately constant, although the deposition time was increased significantly from 60 to 180 min. This may indicate that beyond 60 min of deposition, there is insignificant growth in the films that might have been due to the depletion of the Pb and S ions in the solution.

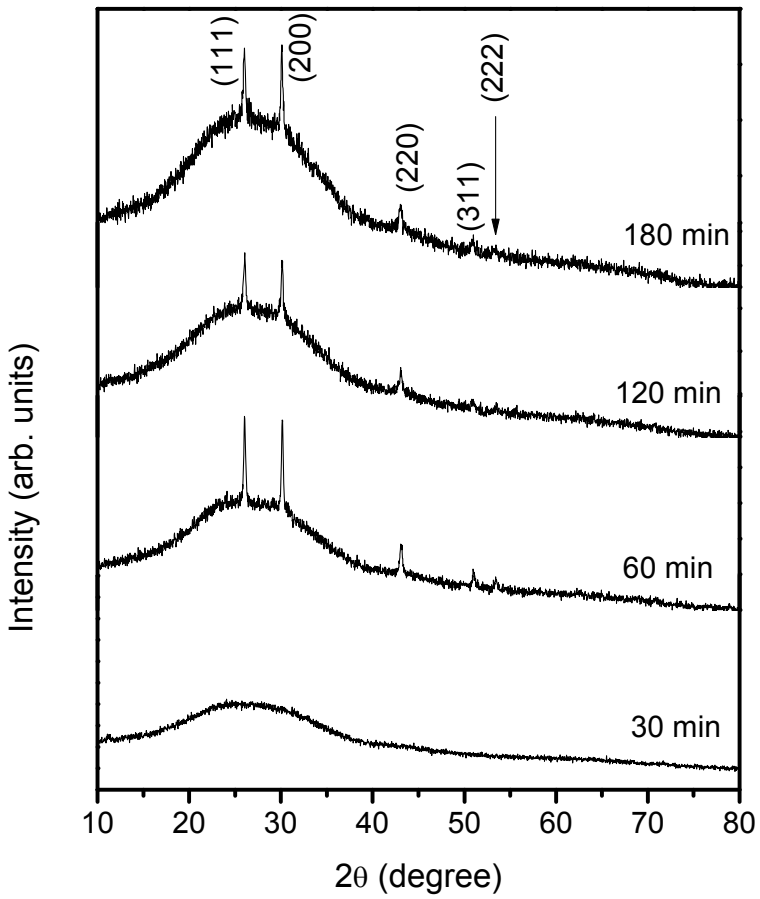

Fig.3. 1: Typical XRD patterns of the PbS thin films grown on glass substrates at a bath temperature of 40 °C for different deposition times.

The crystallite size (t_c) of the films was determined using the Scherrer formula $t_c = 0.9\,\lambda / (\beta \cos\theta)$ where λ is the wavelength of the X-ray radiation (1.54 Å), β is the full-width at the half maximum peak height (FWHM), and 2θ is the Bragg′s angle [92]. The average crystallite size for the films of deposition time of 60 and 120 was determined to be about 30 nm that increased to about 39 nm for the deposition time of 180 min.

3.1.2 SEM studies

Typical surface microstructure of the films grown on glass substrate at 40 °C is shown in **Figure 3.2**. The images on the right panel have been acquired at higher magnification.

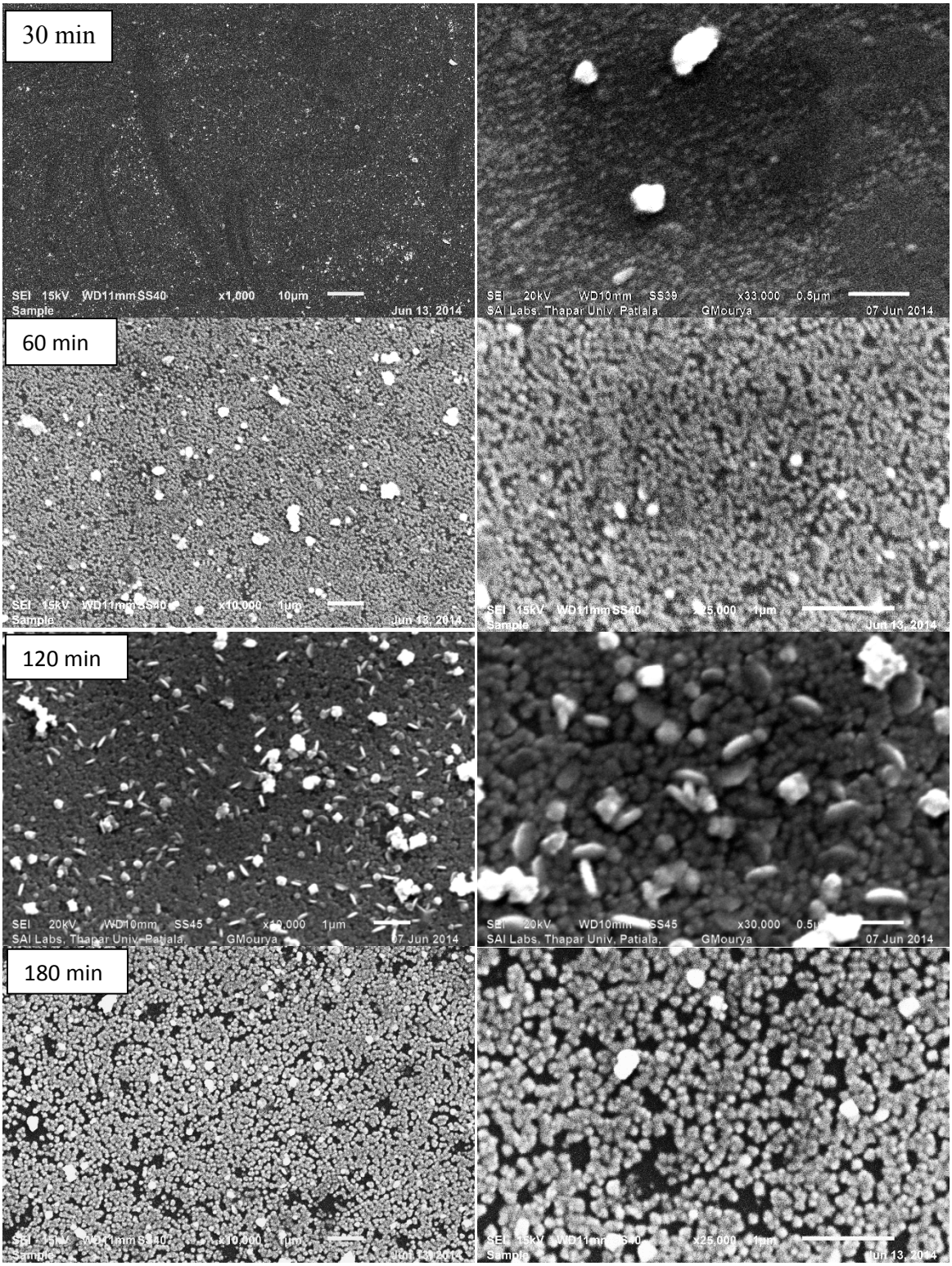

Fig.3. 2: Typical SEM images of PbS thin films prepared at 40 °C for different durations. The images at right panels have been taken at higher magnifications than those in the left panels.

The film prepared for 30 min showed a very thin discontinuous film with the surface covered by extremely small crystallites. As the deposition time was increased, improved coverage of

the substrate by the films was observed. However, it was found that in spite of a very long deposition time (as high as 180 min) the substrate was not fully covered. The films have spherical crystallites whose dimensions increased marginally with increasing deposition time from 60 to 180 min, suggesting that the growth rate has reached the saturation state asymptotically. The results show that it is almost impossible to obtain smooth dense films at 40 °C in a single deposition step.

3.1.3 UV-visible spectroscopy

Typical transmittance spectra for the PbS thin films obtained for different deposition times are presented in **Figure 3.3**. Note that the correction due to the glass substrates has not been made. As observed from the figure, the 30 min film showed very high transparency in the entire wavelength range studied here, similar to the glass substrates (not shown in the figure) owing to its very small thickness and discontinuous nature. As the deposition time was increased to 60 min that resulted in better substrate coverage significant absorption in the range of 300 to 600 nm was observed. The absorption in the lower wavelength region was limited due to the absorption of the glass substrates. With further increase in deposition time yielded pronounced absorption in the entire wavelength region with the maximum transmittance being only 60 %.

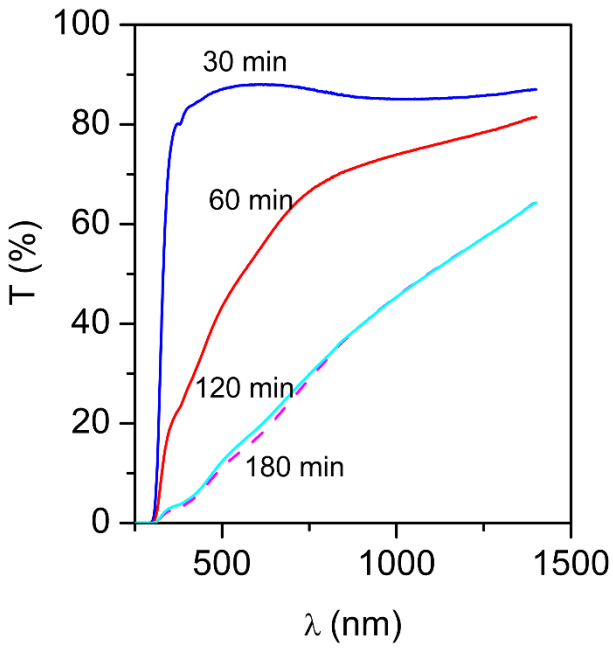

Fig.3. 3: Wavelength dependence of transmittance (%) of the PbS thin films deposited at a bath temperature of 40 °C for different time durations.

The band gap of the films was estimated from the Tauc plots, as described in Chapter 2. Firstly, the absorption coefficient α was determined from the transmittance values (Eq. (2.5)) and $(\alpha h\nu)^2$ was plotted against the photon energy hν. **Figure 3.4** shows such plos for films of various deposition times. The band gap was estimated by extrapolating the linear region of the curves to the zero value of y-axis. For the films of deposition time of 30 and 60 min, it was not possible to estimate band gap of the films due to the non-continuous nature of the films that resulted in high transparency nearer to absorption edge of the glass substrates and the onset of the absorption of the films coincided with that of the substrates.

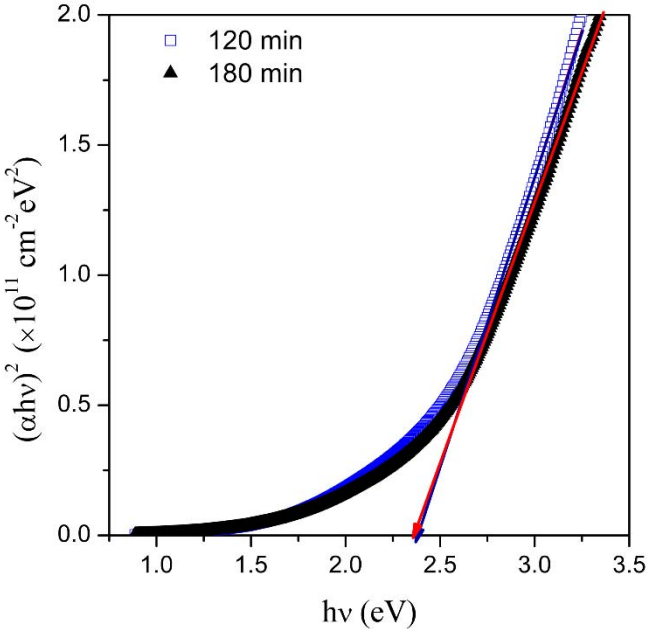

Fig.3. 4: Plot of $(\alpha h\nu)^2$ vs $h\nu$ of the PbS thin films deposited at a bath temperature of 40 °C for different time durations. The arrows indicate extrapolation of the linear regions in the graphs.

The obtained band gap values for the films deposited for 120 and 180 min are listed in **Table 3.1**. These values are much higher than the 0.4 eV reported for the bulk PbS [61]. In literature many authors have reported similar band gaps for films having very small crystallite sizes [93]. It has been attributed the quantum confinement effects. However, in the present case, the crystallite size is in the range of 30-40 nm, as estimated from the analysis of the XRD patterns, which is much higher than the Bohr radius of PbS (~15 nm). Thus, the quantum confinement effect may not be the only reason for the widening of the band gaps. Although it is not clear, the decreasing dimension of the spherical crystallites might have influenced the density of the states resulting in red-shifting the fundamental absorption edge.

Table3. 1: Variation of band gap of the PbS films grown at 40 °C with deposition time.

Deposition time (min)	Band gap (eV)
120	2.38
180	2.37

3.2 Effects of bath temperature on properties of PbS thin films

The results presented in the previous sections indicate that with a single dip, it is almost impossible to obtain a dense film of about 200 nm, which is essential for photovoltaic application. Thus, we have prepared the films at higher bath temperatures, namely at 60 and 80 °C and studied the resulting film properties. The following sections describe the structural, surface morphology and optical properties of the PbS thin films obtained in a single dip at bath temperatures of 60 and 80 °C.

3.2.1 XRD studies

The XRD patterns of the PbS thin films grown on glass substrates at 60 and 80 °C for different deposition times are shown in **Figures 3.5** and **3.6,** respectively. The background comprising of a hump in the range of 20° to 35° has been subtracted for the films deposited at 60 °C. It is observed that for the smallest deposition time of 30 min, the film is well crystallized as evident from multiple peaks in the XRD pattern. The peaks at about 25.86°, 30.10°, 42.92°, 50.96°, 53.28°, 62.35°, 68.76°, 70.73° and 78.73° were identified respectively with (111), (200), (220), (311), (222), (400), (331), (420), and (422) planes of cubic PbS [JCPDS 05-0592].

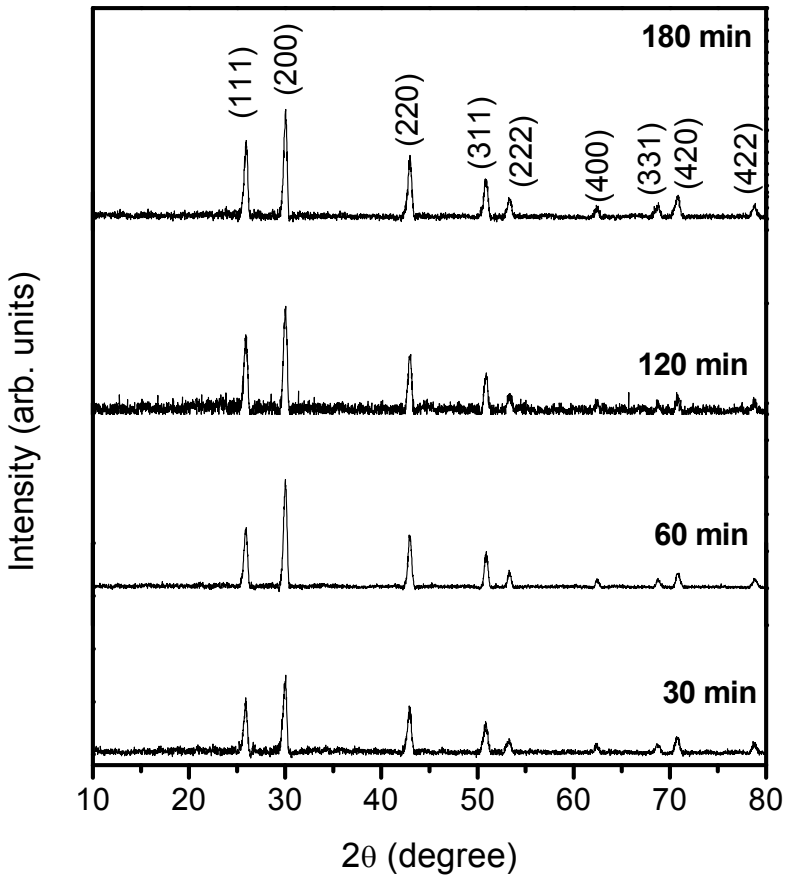

Fig.3. 5: XRD patterns of the PbS thin films deposited at 60 °C for different deposition times.

With increase in the deposition time, the peak width decreased marginally from 0.4035° for 30 min deposition to 0.3491° for 180 min of deposition. This indicates the increase of the crystallite size due to merger of individual smaller crystallites, which may lead to the formation of a continuous film.

For the films deposited at a bath temperature of 80 °C, for a 10 min deposition showed minute peaks corresponding to (111), (200) and (220) planes of cubic PbS. As the time was increased, there was appearance of many sharp peaks indicating improved crystallinity and polycrystalline nature of the films. For the analysis of the evolution of the structural quality, enlarged regions of the XRD patterns are presented in **Fig. 3.7**.

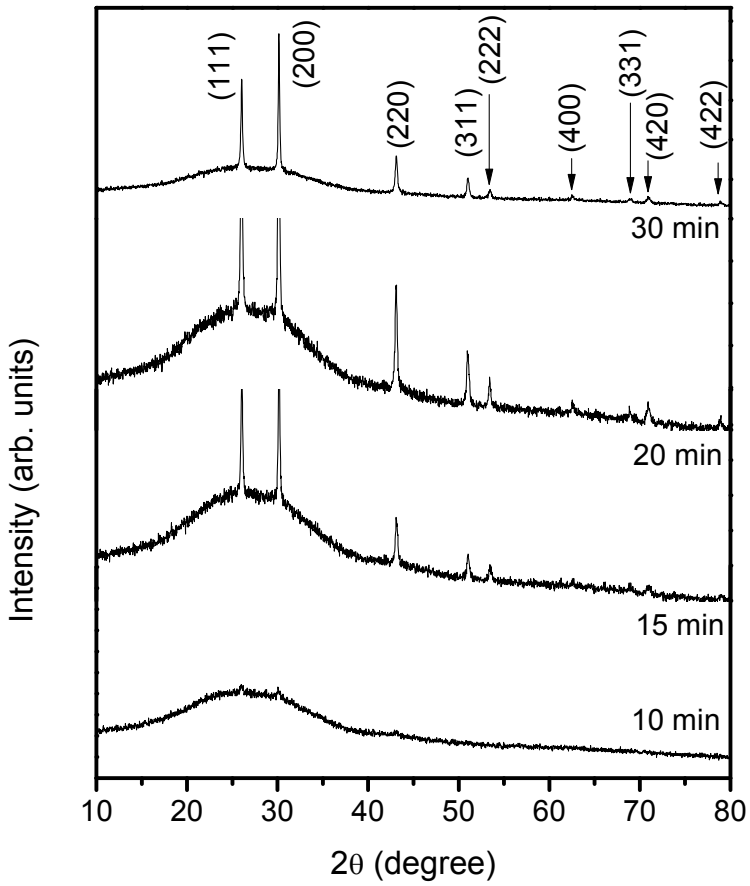

Fig.3. 6: XRD patterns of the PbS thin films deposited at 80 °C for different deposition times.

The evolution of peak intensity and the FWHM of the peaks, namely for the (200) one, was estimated from the Lorentzian fit to the data. From **Fig. 3.7**, it is found that as the deposition increased from 15 to 20 min, intensity of the peaks increased while the FWHM decreased. For example, the intensity of the (200) peak increased from 4000 to 6000 counts while the FWHM decreased from 0.1870° for 15 min deposition time to 0.1698° for 20 min deposition time. However, on further increase of the deposition time, except for the (200) peak, there was no appreciable change in the peak intensities. The FWHM of the (200) peak decreased marginally to 0.1632°. This suggests that beyond, 20 min of deposition, the crystallites tend to grow preferably along the (200) direction.

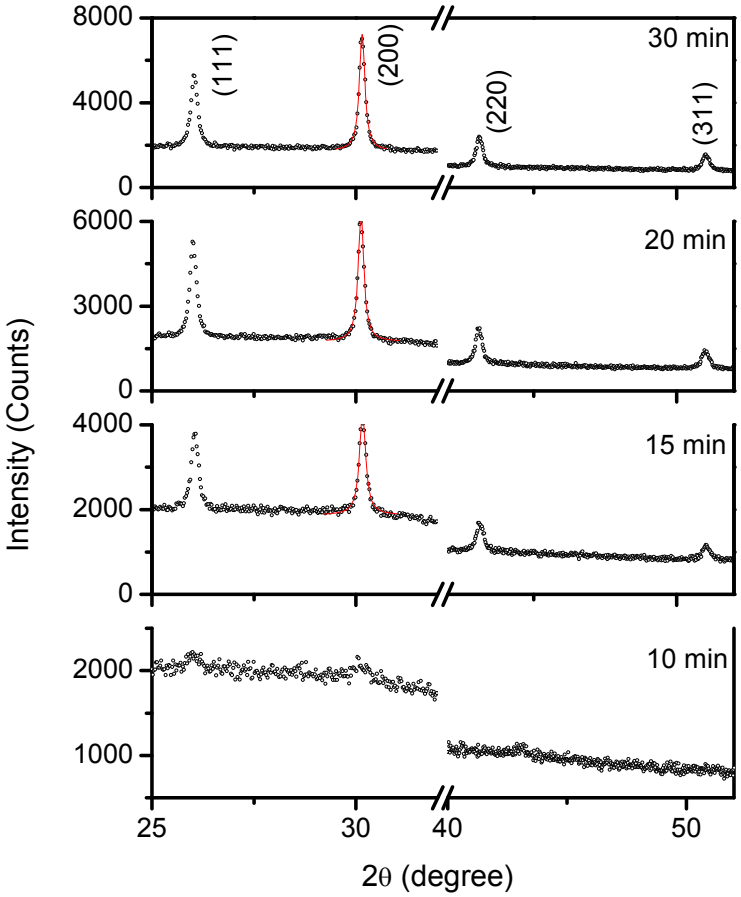

Fig.3. 7: Enlarged regions of the XRD patterns of the PbS thin films grown at 80 °C for different durations. The open circles denote the experimental data and the continuous line (in the region of the (200) peak) is the Lorentz fit to the data points.

3.2.2 SEM studies

Figs. 3.8 and 3.9 depict the evolution of surface microstructures with deposition time for the PbS thin films grown on glass substrates at 60 and 80 °C, respectively. The images on the right panel have been acquired at higher magnification for better clarity. For the 60 °C film, deposition time of 30 min yielded a continuous film with occasional pores. It is observed that over a smooth layer of film of extremely small crystallites, there exist particulates of random shapes of much higher dimensions. With increase in the deposition time, a gradual increase in the crystallite size was observed, which is consistent with the XRD results. In all cases, we observed that particulates of random shapes are present on an otherwise smooth surface. For the film deposition at a bath temperature of 80 °C, even a short duration of 10 min yielded a

dense film (Fig. 3.9). However, the film is not free from pores, although the pores might not extend to the bottom of the films/substrates as revealed from the high magnified SEM images. With increase in deposition time, the pores disappear and the films, however, become rougher with the surface of the film being covered with larger crystallites.

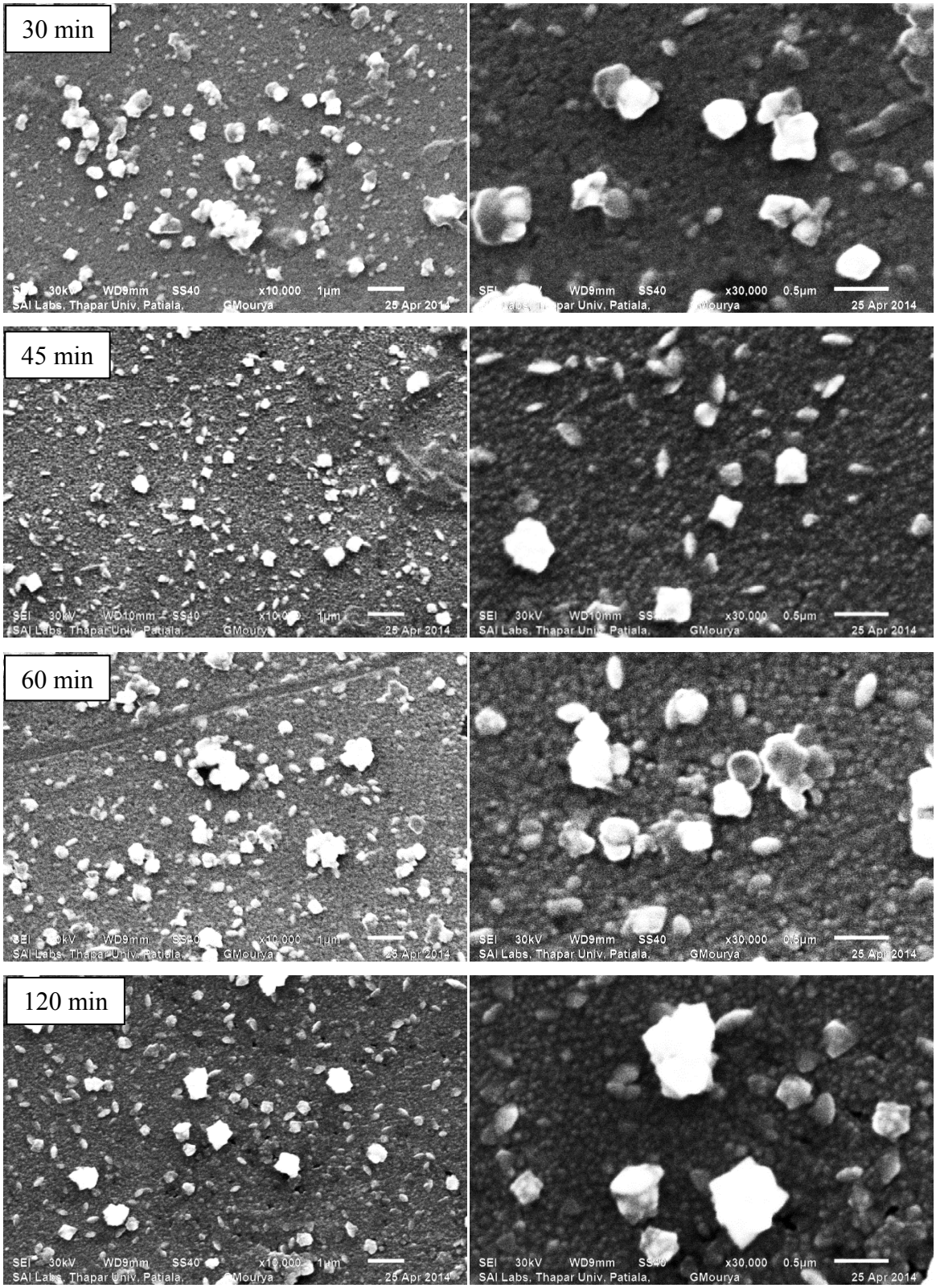

Fig.3. 8: Typical SEM images of PbS thin films prepared at 60 °C for different durations. The images at right panel has been taken at higher magnifications than those in the left panel.

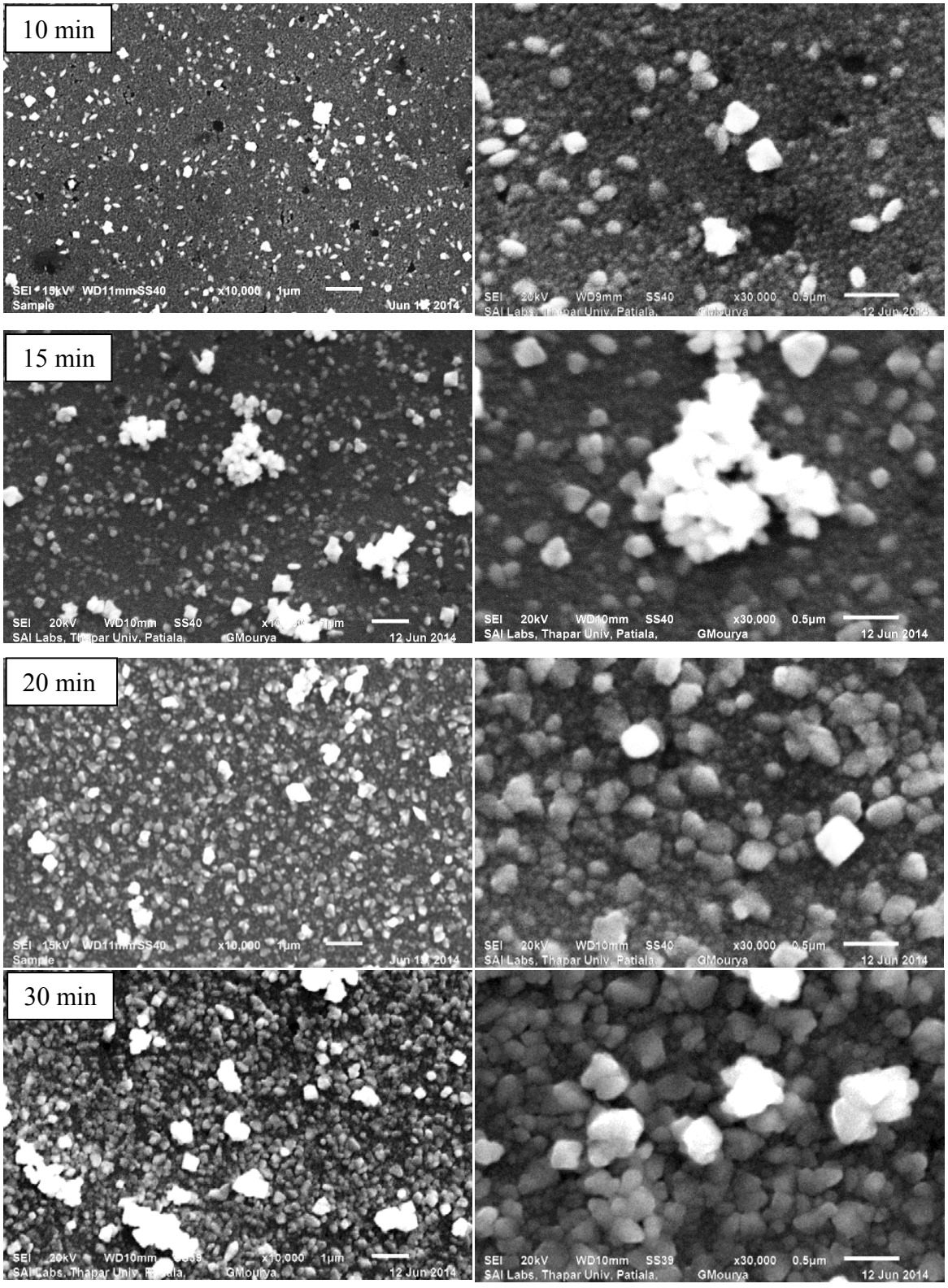

Fig.3. 9: Typical SEM images of PbS thin films prepared at 80 °C for different durations. The images at right panel has been taken at higher magnifications than those in the left panel.

3.2.3 UV-visible spectroscopy

The transmittance spectra for the PbS thin films obtained for different deposition times are presented in **Figs. 3.10 (a)** and **(b)** respectively for the bath temperature of 60 and 80 °C. Note that the correction due to the glass substrates has not been made. For deposition at 60 °C for 30 min (Fig. 3.10a), a low transmittance was observed, the highest being only about 40 %. As the deposition time increased the transmittance gradually decreased. For deposition at 80 °C, similar observations, i.e., decreasing transmittance and blue-shifting of fundamental absorption edge were made.

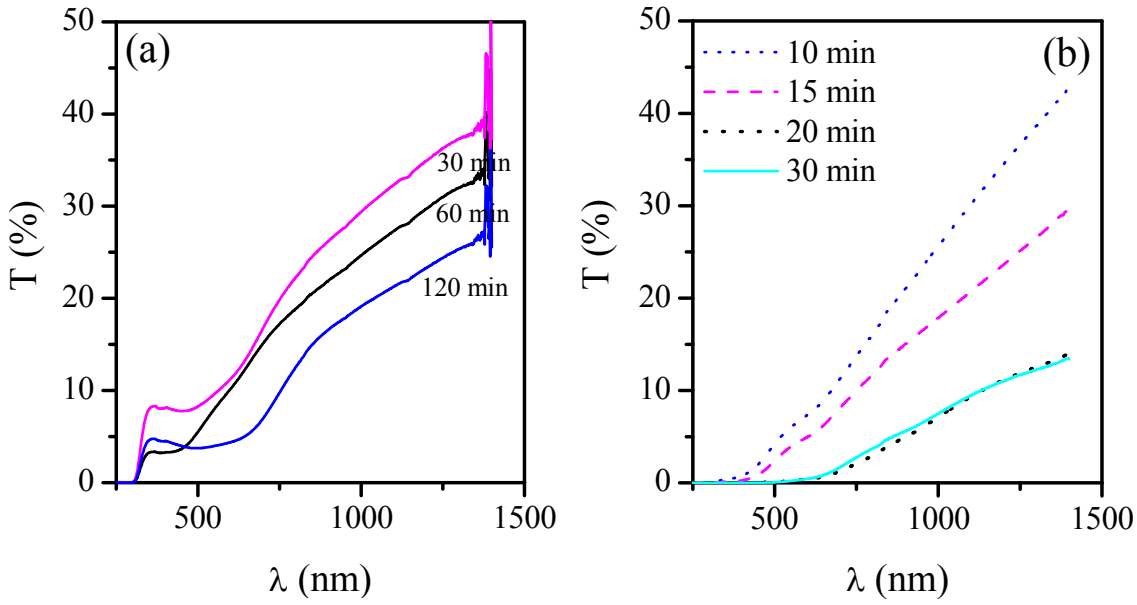

Fig.3. 10: Transmittance (%) curves of the PbS thin films deposited at a bath temperature of (a) 60 and (b) 80°C for different time durations.

As described earlier, the band gap of the films was estimated from the plots of $(\alpha h\nu)^2$ vs $h\nu$. The linear portion of the curves was extrapolated to the zero value of y-axis to determine the band gap. **Figs. 3.11 and 3.12** show the variation of $(\alpha h\nu)^2$ vs the photon energy $h\nu$ for the films deposited for different time durations at 60 and 80 °C, respectively. A linear least-

square fitting was carried out in the linear portion of the curves and was extrapolated (denoted by arrows) to estimate the band gap.

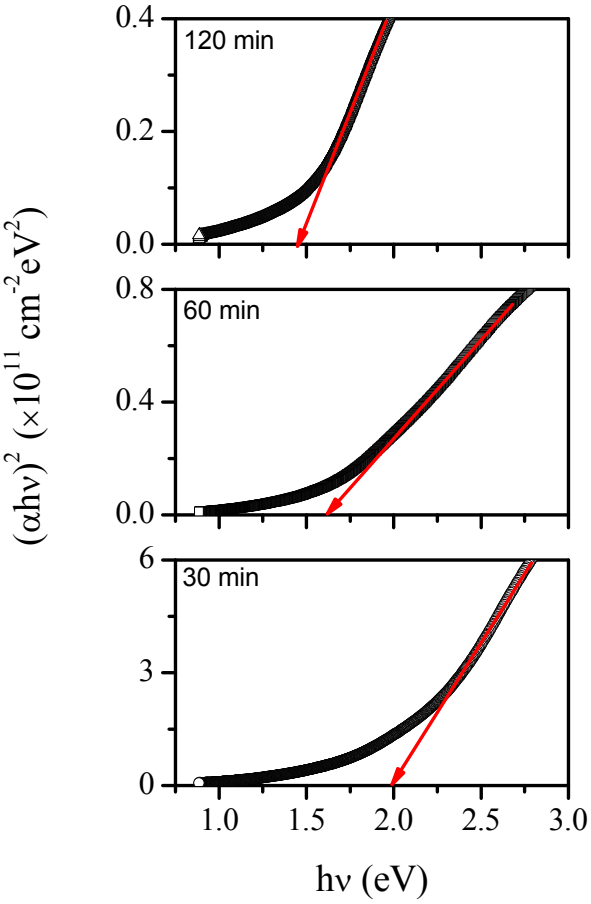

Fig.3. 11: Plot of $(\alpha h\nu)^2$ vs hν of the PbS thin films deposited at a bath temperature of 60 °C for different time durations.

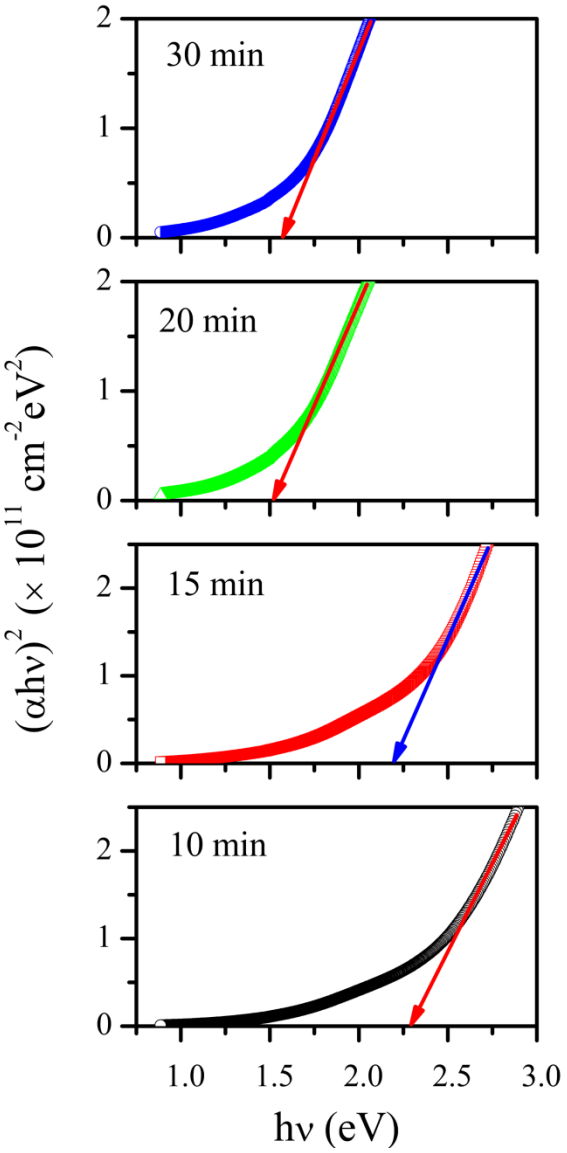

Fig.3. 12: Plot of $(\alpha h\nu)^2$ vs $h\nu$ of the PbS thin films deposited at a bath temperature of 80 °C.

Figures 3.13 (a) and **(b)** show the variation of the band gap with deposition time for the films deposited at 60 and 80 °C, respectively. As expected, the band gap decreased with increase in deposition time for both cases, mainly because of improved crystallite sizes. The thicker films, for example, 60 - 120 min deposition at 60 °C and 20 – 30 min deposition at 80 °C show the band gap values in the range of 1.4 to 1.6 eV, the most preferred one for the photovoltaic applications.

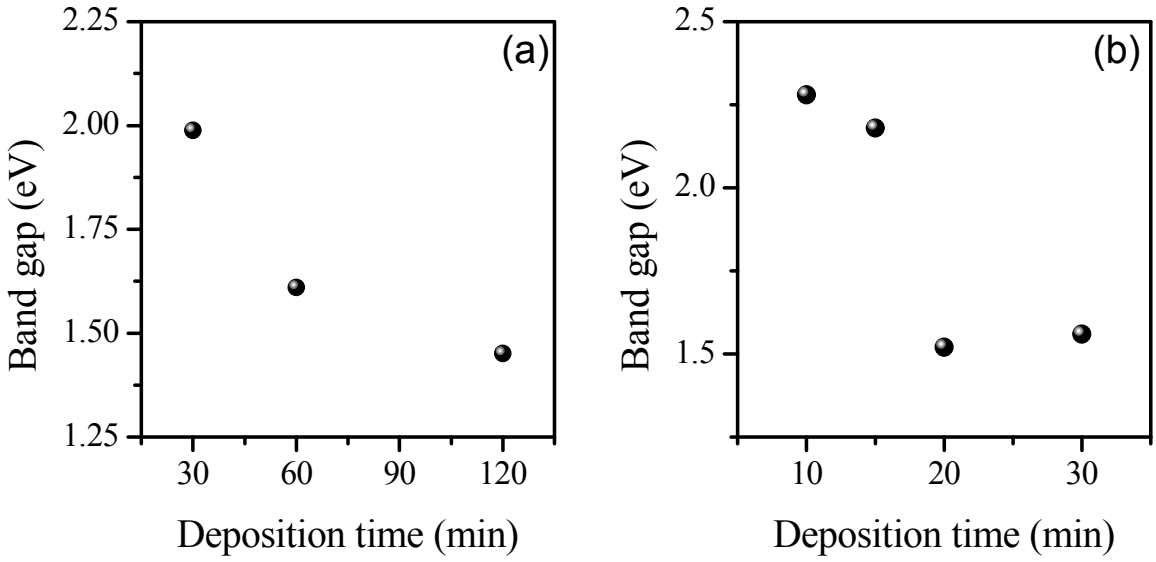

Fig.3. 13: Plot of variation of the band gap with deposition time for the films grown at a bath temperature of (a) 60 and (b) 80 °C.

3.3 Properties of near-room temperature grown CdS thin films

Following the experimental procedures outlined in chapter 2, CdS thin films were prepared by the CBD process at a bath temperature of about 40 °C. In order to determine the thickness suitable for photovoltaic applications, the evolution of film properties with deposition time was studied. In the following sections, the results of the XRD, SEM, AFM and UV-visible spectroscopy studies are presented.

3.3.1 XRD studies

Typical XRD patterns of the CdS thin films grown at a bath temperature of 40 °C for various growth times are presented in **Figure 3.14**. The film of 30 min deposition time shows a very small peak at about 26.8° superimposed on a broad hum in the range of 15 to 35°. The broad hump is due to the glass substrates on which the films were grown. The only peak observed is very close to the (111) plane of the cubic phase of CdS (JCPDS file: 01-080-0019) occurring at 26.547° and (002) peak of hexagonal CdS (JCPDS file: 01-070-2553) occurring at 25.531°.

Considering that the (111) peak of the cubic phase is the highest intensity peak (100% intensity peak) while the (002) peak of the hexagonal phase is only 17.4% intense (the highest intensity peak for the hexagonal phase appears at 28.210° for (101) peak) for the powder samples, and there is no other peak in the XRD pattern of the present film, it is more likely that the crystal structure of the film is cubic. The CBD CdS films exhibiting a strong preferential orientation along the (111) direction is not unusual and the above argument is consistent with the earlier reports.

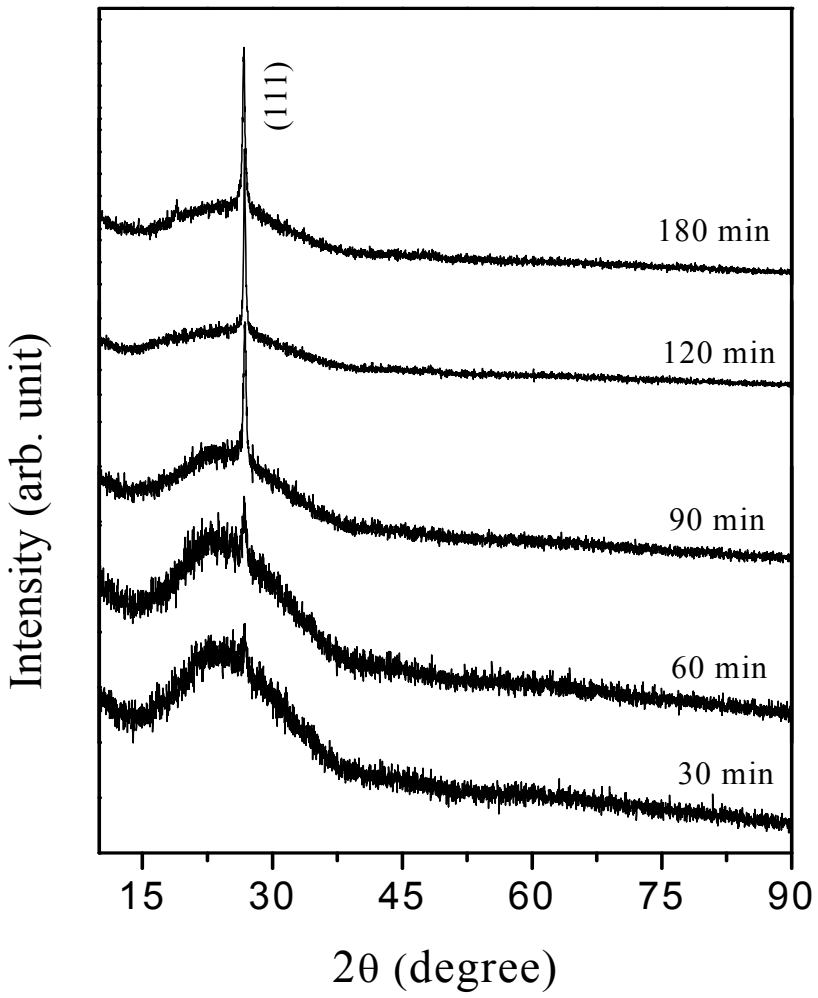

Fig.3. 14: Typical XRD patterns of the CdS thin films deposited at 40 °C for different deposition times.

As the deposition time was increased, there was a gradual increase in intensity of the (111) peak. The peaks become narrower, indicative of improved crystallinity. In literature many researchers have attributed this to the merger of smaller crystallites and growth of the crystallites with simultaneous increase in the film thickness [94-95]. As observed from the **Fig.3.14**, the intensity becomes saturated at about 120 min, indicating that the bath solution gets depleted of the ions at this time and further increasing the deposition time does not yield films of higher thickness or better crystallinity.

3.3.2 SEM studies

Figure 3.15 shows the SEM micrographs depicting surface features of the CdS thin films grown at 40 °C for different durations. By comparing the surfaces of the PbS films deposited at 40 °C (Fig. 3.2), it is observed that the CdS films grew at a faster rate and had a better coverage of the substrate. It may indicate that the release of the cations and anions in the bath composition is slower in the case of PbS compared to CdS. Nevertheless, pores at random places are observed on an otherwise compact surface. As the deposition time was increased, the density of the pores decreased gradually. However, the surface was increasing found to be covered by bigger agglomerates at random places and no correlation of their number with deposition time could be found. Unlike the case of PbS films, it is found that there is progressive change in the surface features indicating that saturation in the growth mode has not been reached despite a long deposition time of 180 min.

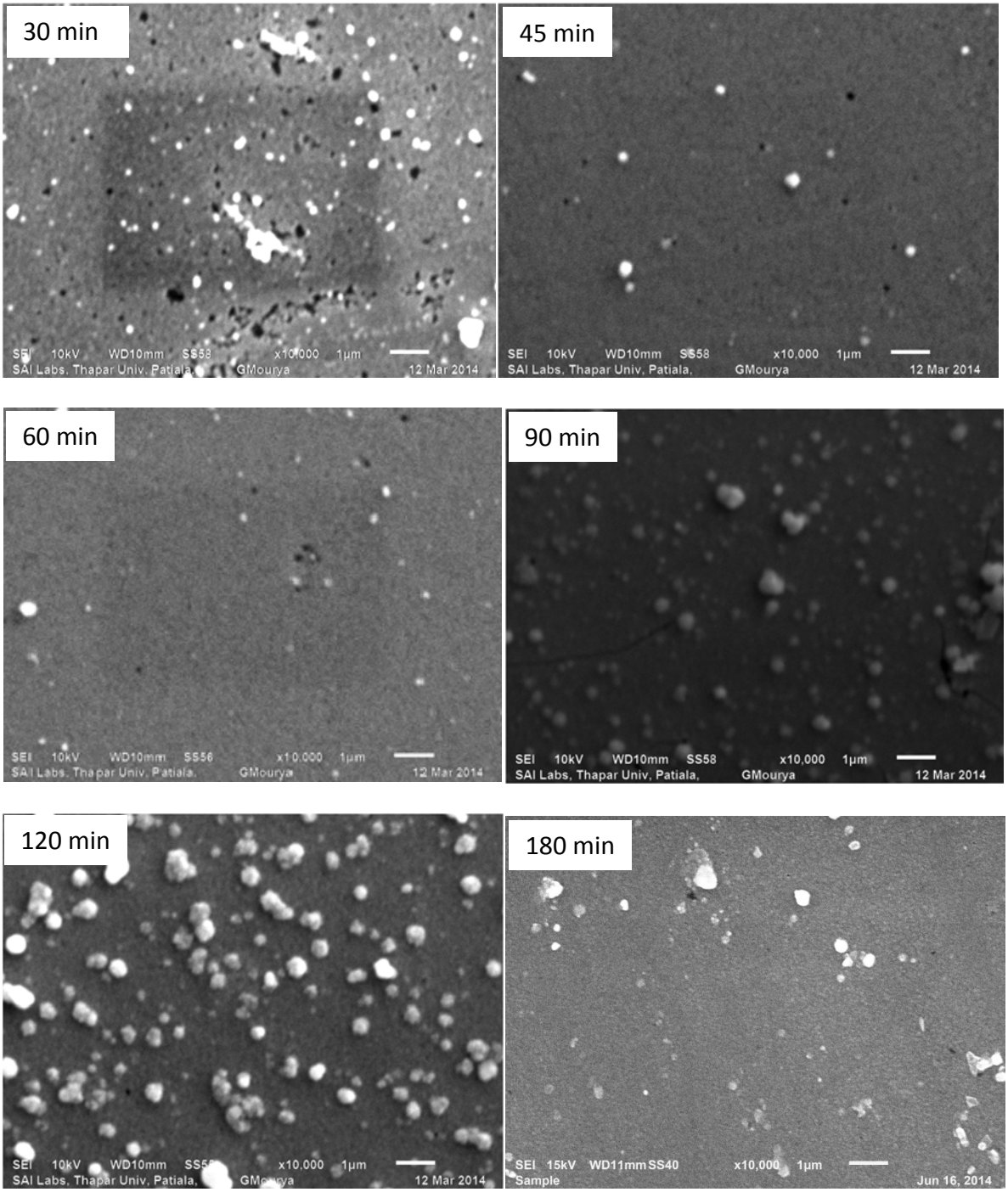

Fig.3. 15: SEM images showing surfaces of CdS thin films deposited at 40 °C for different durations.

3.3.3 AFM studies

Since the SEM images presented in Figure 3.15 reveals the presence of larger particulates on an otherwise smooth surface, AFM was employed to determine the exact nature of the surfaces. Figure 3.16 shows the AFM images of the three dimensional surface topography of

the films at two different scan areas. The left panels show an area of 10 µm × 10 µm while those on the right are of 1 µm × 1 µm. As expected, the larger scan area showed larger crystallites sporadically distributed over the surface area. The smaller scan areas show uniform distribution of size and shape of the crystallites.

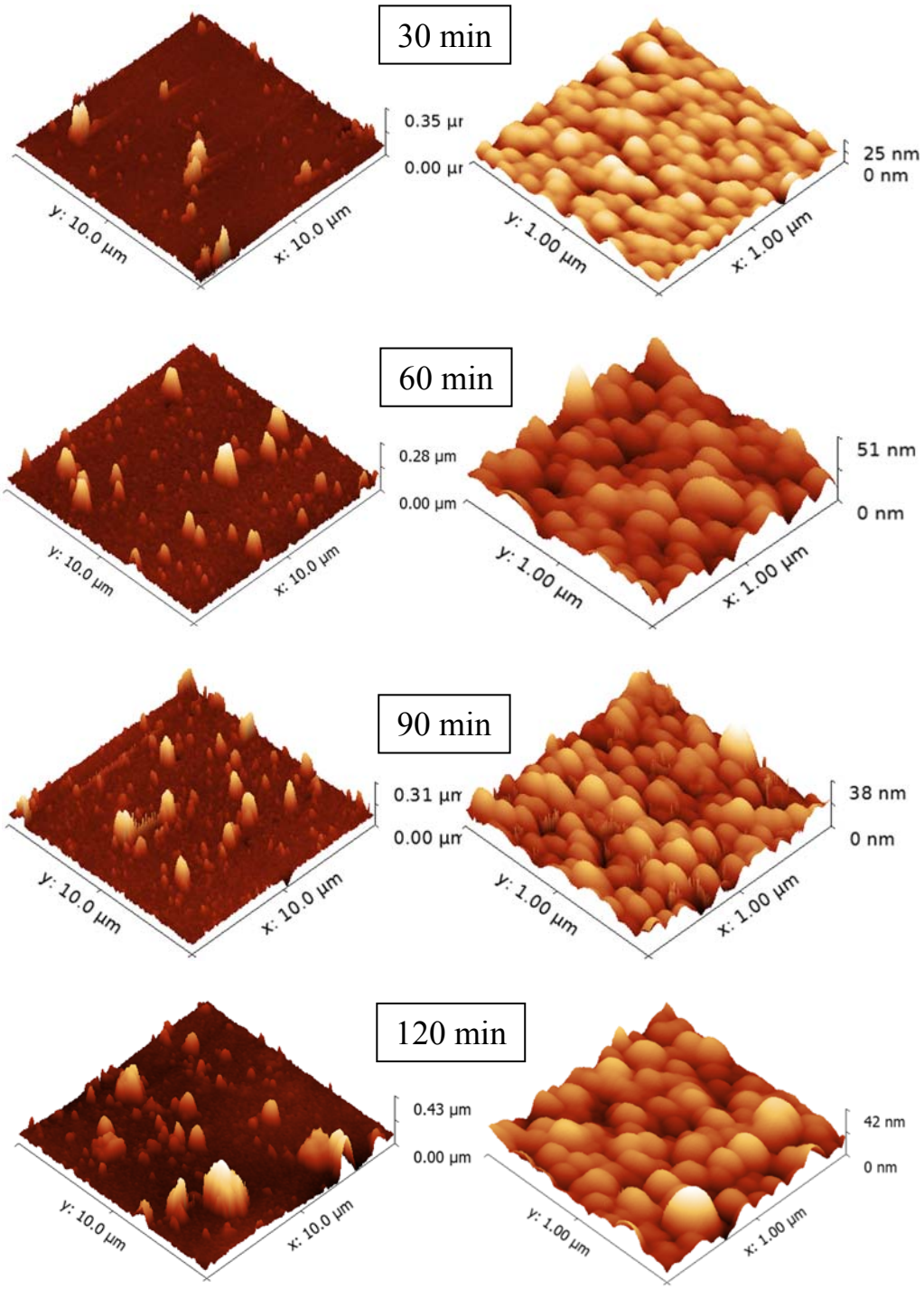

Fig.3. 16: AFM images showing topography of CdS thin films deposited at 40 °C for different durations.

3.3.4 UV-visible spectroscopy

The UV-visible transmittance curves for the CdS thin films grown at a bath temperature of 40 °C for different deposition times are presented in **Figure 3.17**. Note that the correction due to the glass substrates has been made. All films exhibited high transparency in the region of about 500 to 750 nm and the transmittance decreased marginally for wavelengths higher than 800 nm. As can be observed from the figure, fundamental absorption edge is blue-shifted with increase in the deposition time.

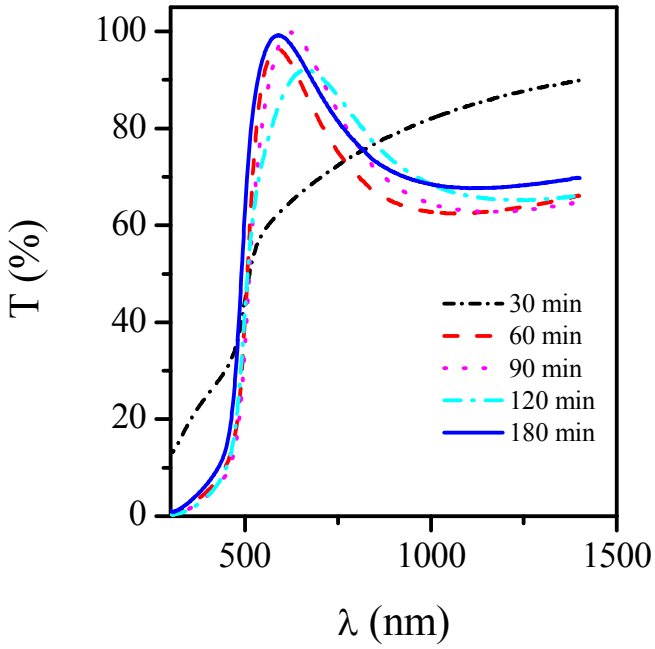

Fig.3. 17: Transmittance spectra of CdS thin films deposited at 40^0 C for different durations

Quantitative evaluation of the band gap was carried out from the Tauc plots, i.e., from the variation of $(\alpha h\nu)^2$ vs hν and extrapolating the linear region. **Figure 3.18** shows the plots of $(\alpha h\nu)^2$ as a function of photon energy for the CdS films of different deposition times.

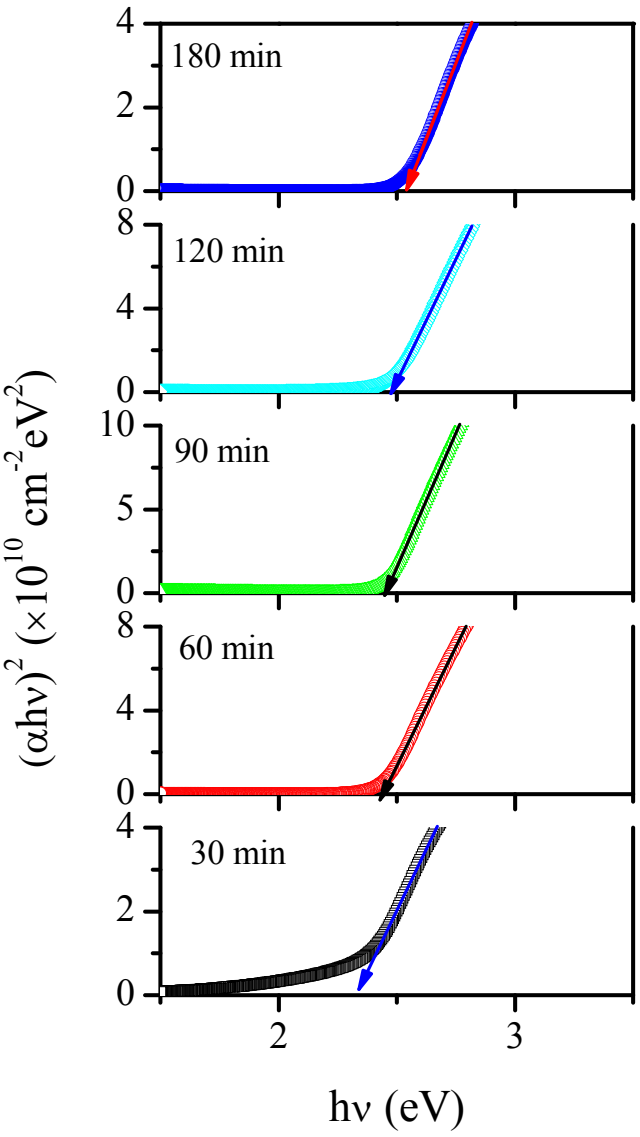

Fig.3. 18: Plot of $(\alpha h\nu)^2$ vs hν for the CdS thin films deposited at a bath temperature of 40 °C for different durations.

The band gap estimated from extrapolation of the linear region to the point of y-axis values zero is plotted in **Fig. 3.19**. The graph shows that gradually the band gap increases from about 2.33 eV to 2.53 eV for increase in deposition time from 30 to 180 min. Although it is not clear, the improved crystallinity and strong preferential growth along the (111) plane may have significant contribution to it.

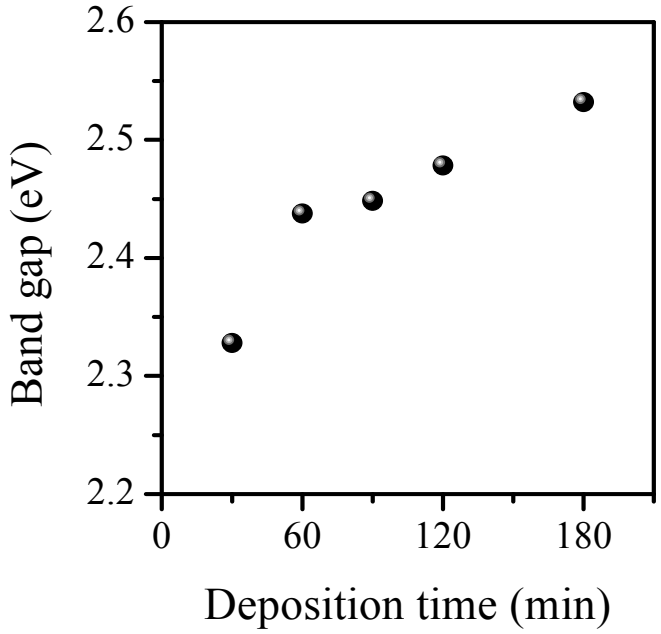

Fig.3. 19: Variation of band gap with deposition time for the CdS thin films grown at 40 °C.

In summary, PbS and CdS thin films were grown on cleaned glass substrates by the CBD process. The effect of deposition time and bath temperature was studied in detail. It was found that for similar bath temperature, the rate of dissociation of reagent compounds in the solution and formation of the compound on the substrate is faster for CdS in compared to PbS. For the PbS films grown at 40 °C, it was not possible to obtain a continuous film in a single dip despite having a deposition time as high as 180 min. However, when the bath temperature was increased to 80 °C, well-adhered continuous films were obtained. On the other hand, growth at 40 °C yielded uniform CdS films that covered the substrate fully in a single dip.

CHAPTER 4

ELECTRICAL CHARACTERIZATION

This chapter deals with the electrical characterization of the PbS/CdS heterojunctions. Firstly, the details of the growth of the heterojunctions and the experimental design for the electrical measurements are presented. The latter portion of the chapter summarizes the results we have obtained.

4.1 Sample preparation for electrical measurement

The CdS and PbS thin films were grown by the CBD process in one dip following the procedures detailed in Chapter 2. Well-cleaned indium tin oxide (ITO)-coated glass substrates of size 2.5 cm × 2.5 cm was used. The ITO coating was used as one of the electrodes during the electrical measurements. The ITO/glass substrates had typical sheet resistances of 10 Ω/□ and very high visible transmittance (better than 80%) in the entire visible spectrum. Since the deposition of CdS thin films at 40 °C for 180 min yielded dense and smooth films with high band gap, all CdS films used for the electrical characterization were grown with the identical process parameters. The PbS thin films were grown at 40, 60 and 80 °C for 180, 90 and 30 min, respectively.

The sample preparation for the electrical characterization includes (i) deposition of CdS on an area of ~1.5 cm × 2.5 cm on the ITO/glass substrates, (ii) deposition of PbS on the area only coated by CdS, and (iii) the contact fabrication by evaporating about 120 nm thick Al through masks. Details have been provided in Chapter 2. **Fig. 4.1** shows the schematics of the process steps of sample preparation. In some cases, a 1 nm-thick LiF was thermally evaporated following the literature that LiF/Al is an alternate contact to Al. Two of the actual

photographs have been presented in **Chapter 2.** J – V measurements were carried out on the following structures: (i) Glass/ ITO/ PbS/ LiF/ Al, (ii) Glass/ ITO/ PbS/ Al, (iii) Glass/ ITO/ CdS/ PbS/ LiF/Al and (iv) Glass/ ITO/ CdS/ PbS/ Al. The intention of such structures was to evaluate the performance of Schottky junction between the PbS with metals while that of the last two ones was to assess the photovoltaic performances. The light was made incident from the substrate side.

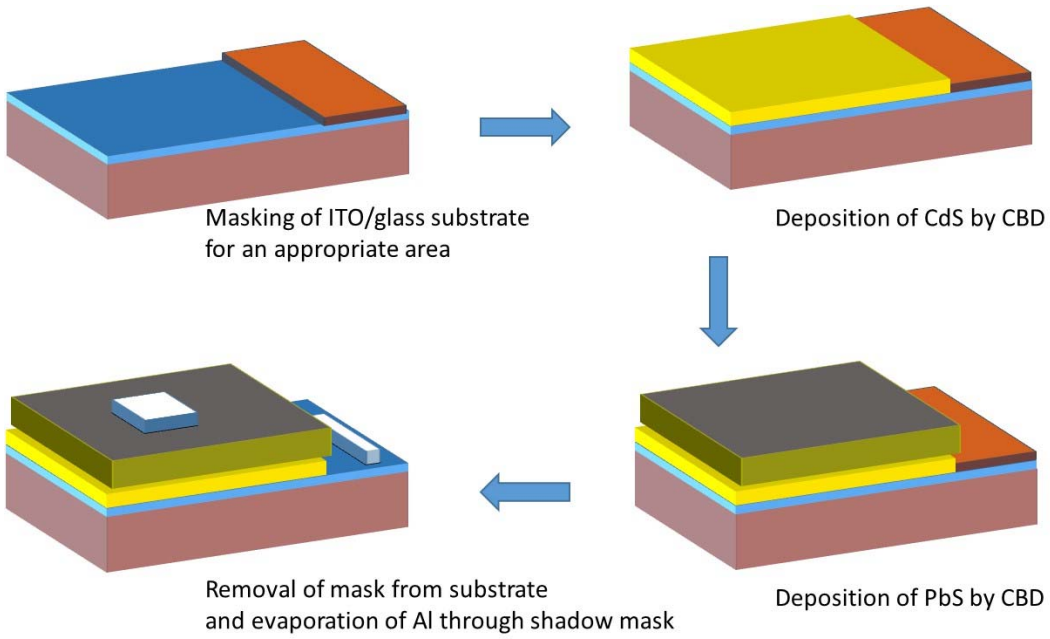

Fig.4. 1: Schematics of preparation of samples for electrical characterization

4.2: Results and discussion

Fig. 4.2 shows the typical J-V characteristics of the Schottky junctions of the structure ITO/PbS/Al and ITO/PbS/LiF/Al in the dark condition. The PbS films grown at 40 °C for 180 min for the maximum possible thickness, as presented in Chapter 3. The notations Al and LiF/Al indicate the cases where Al or LiF/Al were prepared as top contacts. As the graph shows, linear behavior was obtained for at least 10 junctions, indicating that the junction is

short-circuited. This behavior typically arises when the top and bottom electrodes come in direct contact mainly because of physical failure of the interlayers (PbS in this case). The PbS films grown at 40 and 60 °C for all deposition times showed numerous pores/holes, as revealed from the SEM images (presented in Chapter 3). This could be the main reason for the observed J-V behavior. Based on this observation, further electrical characterization was carried out only on the 80 °C - PbS films.

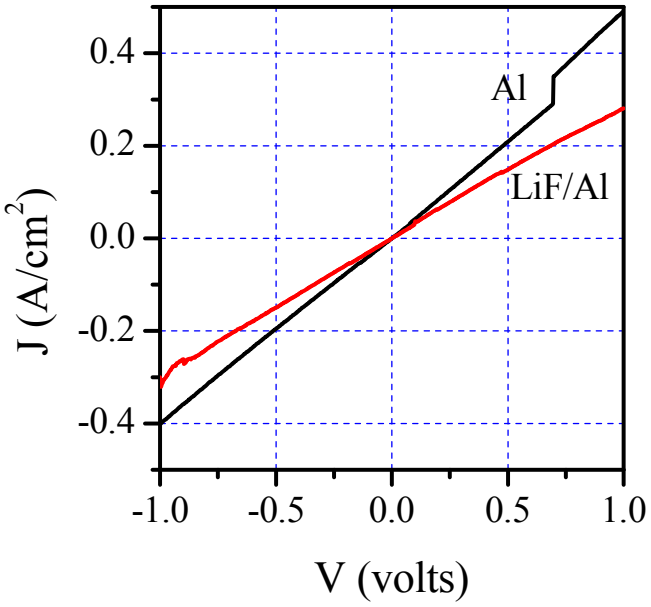

Fig.4. 2: Typical dark J-V characteristics of the junctions of structure ITO/PbS/Al and ITO/PbS/LiF/Al.

The J-V characteristics of the Schottky junctions based on PbS thin films grown at 80 °C for 30 min are shown in **Fig. 4.3**. A clear non-linear behavior is observed from the figure for both dark and illuminated (simulated sun light of intensity 100 mW/cm^2) conditions. For both forward and reverse bias, significant light current was observed compared to the dark one. For instance, at a reverse bias of 0.5 V, a difference of about 1.2 mA/cm^2 in the current density could be obtained. However, no photovoltaic response was obtained.

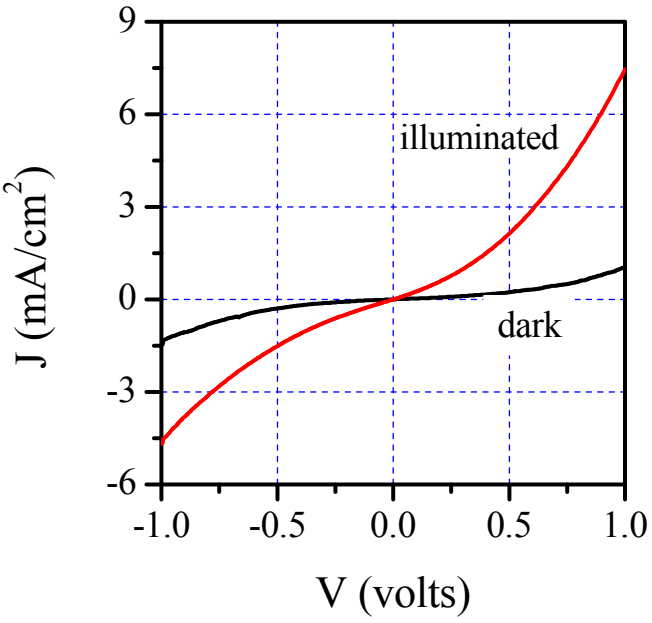

Fig.4. 3: Typical J-V characteristics of the junctions of structure ITO/PbS/Al. The PbS films were grown at a bath temperature of 80 °C.

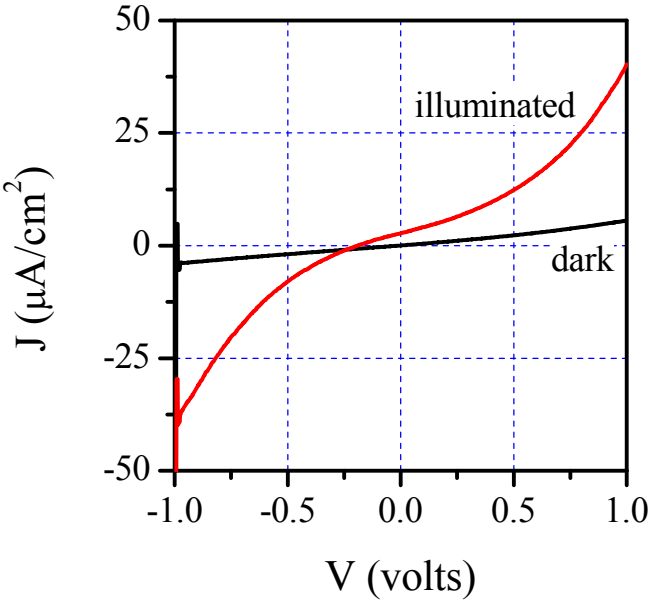

Fig.4. 4: J-V characteristics of the junctions of structure ITO/CdS/PbS/Al.

The current density - voltage (J-V) characteristics of the diodes of the structure ITO/CdS/PbS/Al are shown in **Fig. 4.4**. As mentioned before, the PbS thin films were grown at 80 °C for 30 min, while the CdS films were prepared at 40 °C for 180 min. As seen in **Fig.**

4.4, the diode indicates a rectifying contact between n-CdS and p-PbS. As the junction was irradiated, the current density values and shape of the J-V curve was significantly changed for both forward and reverse bias. The curves obtain at a solar radiation of 100 mW/cm^2 was oddly asymmetric with a current density of about 3 $\mu A/cm^2$ at zero bias. It was found that photocurrent to dark current contrast ratios of the junctions was about 6.3 and 9.5 respectively for forward and reverse biasing at 1 V. The low current contrast ratio is possibly due to imperfections of the heterojunction interface traps between the CdS and the PbS films. It is worth noting that a set of 10 junctions, which were prepared under identical conditions, showed similar behavior, i.e., a positive current density at V = 0. With this J-V curve under illumination it was not possible to evaluate the photovoltaic performance of the junctions. Upon improving quality of the films, any energy conversion efficiency may be expected from such heterojunctions.

CHAPTER 5

SUMMARY AND FUTURE SCOPE

PbS and CdS thin films were grown by the CBD process. Since the control of process parameters is relatively easier, this technique has been traditionally used in deposition of thin films of many technologically important materials. Furthermore, it requires inexpensive setup and films using the process can be deposited over a large area. Thus, the CBD technique has been well-accepted as industry-friendly. During the process, among various parameters, the deposition time is crucial in the CBD process. Unlike the vacuum deposition techniques such as evaporation or sputtering which has a constant source of depositing species, in the CBD process controlling the thickness of the films in the CBD process is complicated. During the deposition in the CBD process, the source ions get depleted with deposition time and thus, for a given starting concentration of the bath solution, the deposition rate saturates with deposition time. In this work, it was attempted to prepare the films were grown for different durations and their properties were examined for possible photovoltaic applications.

Since from the industry point of view, fabrication of the devices at low temperatures is desirable for minimizing the thermal cost, it was intended to prepare the films at room temperature. However, it was found that no film could be deposited at ~30 °C, in spite of a very long deposition time. When the bath temperature was increased to about 40 °C, films could be successfully deposited, however. The evolution of film properties with deposition time was investigated using a variety of techniques such as XRD, SEM, AFM, UV-visible spectroscopy.

For the PbS films, it was found that for a bath temperature of 40 °C, the films exhibited numerous holes and it was not possible to obtain a dense film of about 200 nm, which is essential for photovoltaic application, despite a deposition time as long as 180 min. Thus, a higher bath temperature, namely at 60 and 80 °C was used and properties of the resulting films were evaluated. Typically it was found that with increase in deposition time, crystallinity of the films improved, as expected. For long deposition times, PbS films exhibited polycrystalline nature, characterized by sharp XRD peaks. The band gap of the films also showed strong dependence on the bath temperature as well as deposition time. The thicker films, for example, 60 - 120 min deposition at 60 °C and 20 – 30 min deposition at 80 °C show the band gap values in the range of 1.4 to 1.6 eV, the most preferred one for the photovoltaic applications.

Compared to the PbS thin films, it was found that for similar bath temperature, the rate of dissociation of reagent compounds in the solution and formation of the compound on the substrate is faster for CdS. While for the PbS films grown at 40 °C, it was not possible to obtain a continuous film in a single dip despite having a deposition time as high as 180 min, growth at 40 °C yielded uniform CdS films that covered the substrate fully in a single dip. The band gap of the CdS films for a deposition time ranging from 30 to 160 min was in the range of 2.3 to 2.6 eV.

Hall measurement of the films showed that Pbs films were p-type in nature while CdS films showed n-type conductivity. Schottky and heterojunctions of the structures ITO/PbS/Al and ITO/CdS/PbS/Al were formed and their current density – voltage curves were obtained. It was found that although PbS (80 °C)/Al junctions showed Schottky behavior, a meaningful photovoltaic response could not be observed, possible because of inferior quality of the films.

Based on the results of this work, it is believed that multiple dips will improve the quality of the films, especially the microstructure and hence, the electrical transport characteristics. The effects of other process parameters such as ion concentrations, pH of the solution, etc on the growth rate of the films can be monitored to optimize the film properties. Although in this work, any post deposition heat treatments was not carried out, it will be of interest to find out the effects of thereof. The above listed experiments can further our understanding and help achieving photovoltaic devices of better performance.

References

[1] K. L. Chopra, “Thin Film Solar Cells,” *Mc-Graw Hills* (1983).

[2] D. Smith, “Thin Film Deposition: Principle and Practice,” *Mc-Graw Hills* (1995).

[3] P. Bhattacharya, “Semiconductor Optoelectronic Devices”, *Prentice Hall India* (2009).

[4] L. Yu, Y. Lv, G. Chen, X. Zhang, Y. Zeng, H. Huang and Y. Feng, "A Generally Synthetic Route to Semiconducting Metal Sulfide Nanocrystals by Using Corresponding Metal Powder and Cysteine as Metallic and Sulfuric Sources, respectively," *Inorg. Chim. Acta,* **376**, 659 (2011).

[5] J. S. Steckel, J. P. Zimmer, S. Coe-Sullivan, N. E. Stott, V. Bulović and M. G. Bawendi, "Blue Luminescence from (CdS) ZnS Core–Shell Nanocrystals," *Angew. Chem. Int. Ed.,* **43**, 2154 (2004).

[6] A. Fu, W. Gu, B. Boussert, K. Koski, D. Gerion, L. Manna, M. Le Gros, C. A. Larabell and A. P. Alivisatos, "Semiconductor Quantum Rods as Single Molecule Fluorescent Biological Labels," *Nano Lett.,* **7**, 179 (2007).

[7] Z. Zhuang, X. Lu, Q. Peng and Y. Li, "A Facile “Dispersion–Decomposition” Route to Metal Sulfide Nanocrystals," *Chem. -Eur. J.,* **17**, 10445 (2011).

[8] W. Scanlon,” Intrinsic Optical Absorption and the Radiative Recombination Lifetime in PbS” *Phys. Rev*., **106**, 718 (1957).

[9] O. Savadogo and K. C. Mandel, “Formation of Antimony Sulphide Powders and Thin Films from Single Source Antimony Precursors,” *Sol. Energy Mater. Sol. Cells*, **26**, 117 (1992).

[10] A. Wachtel and A. Noreika,” Growth and Characterization of CuS Crystals,” *J.Electron. Mater.,* **9**, 281 (1980).

[11] P. Pramanik, P.K. Basu, and S. Biswas, “Chemical Deposition Method for Metal Chalcogenide Thin Films” *Thin Solid Films,* **150**, 269 (1987).

[12] H. Feng, J. Wang, W. Fan, and C. Zhang,” Highly Uniform Matchstick-like Ag_2S–ZnS Hetero-nanorods using Dodecanethiol as a Sulfur Source”, *Materials Letters,* **126**, 67 (2014).

[13] G. Hodes, “Chemical Solution Deposition of Semiconductor Thin Films”, *Marcel Dekker*, 190 (2003).

[14] N. Tessler, V. Medvedev, M. Kazes, S. Kan, and U. Banin, “Efficient Near-infrared Polymer Nanocrystal Light-emitting Diodes,” *Science*, **295**, 1506 (2002).

[15] A.G Milnes and A.Y Polyakov,” Indium Arsenide: A Semiconductor for High Speed and Electro-Optical Devices,” *Materials Science and Engineering,* **18**, 237(1993).

[16] A. Antony, K.V. Murali, R. Manoj and M.K. Jayaraj,”Preparation and Characterisation of ZnS Thin Films by Chemical Bath Deposition,” *Mater. Chem. Phys.***90,** 106 (2005).

[17] G. JeffreyaSnyder, "High Thermoelectric Figure of Merit in Heavy Hole Dominated PbTe," *Energy Environ. Sci.,* **4**, 2085 (2011).

[18] S. Ovsyannikov, V. Shchennikov, S. Popova and A. Y. Derevskov, "Semiconductor–Metal Transitions in Lead Chalcogenides at High Pressure," *Phys. Status Solidi B-Basic Solid State Phys.,* **235**, 521 (2003).

[19] C. Wadia, A. P. Alivisatos and D. M. Kammen, "Materials Availability Expands the Opportunity for Large-Scale Photovoltaics Deployment," *Environ. Sci. Technol.,* **43**, 2072 (2009).

[20] A. E. Pop, V. Popescu, M. Danila and M. N. Batin, "Optical Properties of Cu_xS Nano-Powders," *Chalcogenide Lett.,* **8**, 36 (2011).

[21] K. Okamoto and S. Kawai, "Electrical Conduction and Phase Transition of Copper Sulfides," *Jpn. J. Appl. Phys.,* **12**, 1130 (1973).

[22] S. Wang, J. Zhang, Y. Zhang, A. Alvarado, J. Attapattu, D. He, L. Wang, C. Chen and Y. Zhao, "Phase-Transition Induced Elastic Softening and Band Gap Transition in Semiconducting PbS at High Pressure," *Inorg. Chem.,* **52**, 8638 (2013).

[23] P. P. Boix, G. Larramona, A. Jacob, B. Delatouche, I. Mora-Sero and J. Bisquert, "Hole Transport and Recombination in All-Solid Sb_2S_3-Sensitized TiO_2 Solar Cells Using CuSCN as Hole Transporter," *J. Phys. Chem. C,* **116**, 1579 (2011).

[24] A. R. West," Basic Solid State Chemistry," *John Wiley and Sons* (1999).

[25] K. L. Chopra, P. D. Paulson and V. Dutta, "Thin-Film Solar Cells: An Overview," *Prog. Photovolt: Res. Appl.,* **12**, 69 (2004).

[26] V. Fthenakis, "Sustainability of Photovoltaics: The Case for Thin-Film Solar Cells," *Renew. Sust. Energ. Rev.,* **13**, 2746 (2009).

[27] J. Grigas, E. Talik and V. Lazauskas, "X-ray Photoelectron Spectra and Electronic Structure of Bi_2S_3 Crystals," *Phys. Status Solidi B-Basic Solid State Phys.,* **232**, 220 (2002).

[28] H. Pathan and C. Lokhande, "Deposition of Metal Chalcogenide Thin Films by Successive Ionic Layer Adsorption and Reaction (SILAR) Method," *Bull. Mater. Sci.,* **27**, 85 (2004).

[29] U. Jadhav, M. Shinde, S. Patel and R. Patil, "Structural, Optical and Electrical Properties of Nanocrystalline Cadmium Sulphide Thin Films Deposited by Novel Chemical Route," *Indian J. Pure Ap. Phy.,* **52**, 39 (2014).

[30] H. Khallaf, G. Chai, O. Lupan, L. Chow, S. Park and A. Schulte, "Characterization of Gallium-Doped CdS Thin Films Grown by Chemical Bath Deposition," *Appl. Surf. Sci.,* **255**, 4129 (2009).

[31] S. Ramprasad, Y.-W. Su, C. Chang, B. K. Paul and D. R. Palo, "Cadmium Sulfide Thin Film Deposition: A Parametric Study Using Microreactor-Assisted Chemical Solution Deposition," *Sol. Energy Mater. Sol. Cells,* **96**, 77 (2012).

[32] K. P. Bhandari, P. J. Roland, H. Mahabaduge, N. O. Haugen, C. R. Grice, S. Jeong, T. Dykstra, J. Gao and R. J. Ellingson, "Thin Film Solar Cells Based on The Heterojunction of Colloidal PbS Quantum Dots with CdS," *Sol. Energy Mater. Sol. Cells,* **117**, 476 (2013).

[33] S.M. Pawar, B.S. Pawar, J.H. Kim, Oh-Shim Joo and C.D. Lokhande," Recent Status of Chemical Bath Deposited Metal Chalcogenide and Metal Oxide Thin Films", *Current Applied Physics*, **11**, 120 (2011).

[34] G. Hodes," Chemical Solution Deposition of Semiconductor Thin Films", *Marcel Dekker*, (2003).

[35] I. Pop, C. Nascu, V. Ionescu, E. Indrea and I. Bratu," Structural and Optical Properties of PbS Thin Films Obtained by Chemical Deposition," *Thin solid films,* **307**, 240 (1997).

[36] R.S. Patil, H.M. Pathan, T.P. Gujar and C.D. Lokhande," Characterization of Chemically Deposited Nanocrystalline PbS Thin Films," *J. Mater. Sci.*, **41,** 5723 (2006).

[37] S. Seghaier, N. Kamoun, R. Brini and A.B. Amar," Structural and Optical Properties of PbS Thin Films Deposited by Chemical Bath Deposition Technique," *Mater. Chem. Phys*., **97**, 71 (2006).

[38] A. Osherov, M. Shandalov, V. Ezersky and Y. Golan," EPITAXY and Orientation Control in Chemical Solution Deposited PbS and PbSe Monocrystalline films,"*J. Cryst. Growth*, **304**, 169 (2007).

[39] S. Jana, R. Thapa, R. Maity and K. K. Chattopadhyay," Optical and Dielectric Properties of PVA Capped Nanocrystalline PbS Thin Films Synthesized By Chemical Bath Deposition," *Physica E,* **40**, 3121 (2008).

[40] L. Raniero, C. L. Ferreira, L. R. Cruz, A.L. Pinto and R.M.P. Alves," Photoconductivity Activation in PbS Thin Films Grown at Room Temperature by Chemical Bath Deposition*" physica B*, **45**, 1283 (2010).

[41] M.M. Abbas, A. Ab-M. Shehab, N-A. Hassan and A-K. Al-Samuraee, "Effect of Temperature and Deposition Time on the Optical Properties of Chemically Deposited Nanostructure PbS Thin Films," *Thin Solid Films,* **519**, 4917 (2011).

[42] A.S. Obaid, M. A. Mahdi, Z. Hassan and M. Bououdina," Characterization of Nanocrystalline PbS Thin Films Prepared using Microwave-Assisted Chemical Bath Deposition," *Materials Science in Semiconductor Processing,* **15**, 564 (2012).

[43] T. Tohidi, K. Jamshidi- Ghaleh, A. Namdar and R. Abdi- Ghaleh, "Comparative Studies on the Structural, Morphological, Optical, and Electrical Properties of Nanocrystalline PbS Thin Films Grown by Chemical Bath Deposition using Two Different Bath Compositions," *Materials Science in Semiconductor Processing,* **11**, 100 (2013).

[44] B. Altiokka, M. Celalettin Baykul and M. Riza Altiokka, "Some Physical Effects of Reaction Rate on PbS Thin Films Obtained by Chemical Bath Deposition," *Journal of Crystal Growth,* **384**, 52 (2013).

[45] K. C. Preetha and T. L. Remadevi," Optimization of PbS Thin Films Using Different Metal ion Sources for Photovoltaic Applications," *J Material Sci: Mater Electron*, **24**, 489 (2013).

[46] J.A. Garcia-Valenzuela, M.R. Baez-Gaxiola and M. Sotelo-Lerma, "Chemical Bath Deposition of PbS Thin Films on Float Glass Substrate Using a $Pb(CH_3COO)_2$-NaOH-$(NH_2)_2CS$-$N(CH_2CH_2OH)_3$-CH_3CH_2OH Definite Aqueous System and Their Structural, Optical and Electrical/Photoelectrical Characterization," *Thin Solid Films,* **534**, 126 (2013).

[47] F. Gode, E. Guneri, F. M. Emen, V. Emir Kafadar and S. Unlu," Synthesis, Structural, Optical, Electrical and Thermo luminescence Properties of Chemically Deposited PbS Thin Films," *Journal ofLuminescence,***147**, 44 (2014).

[48] J. Herrero, M.T. Gutiearrez, C. Guillean, J.M. Dona, M.A. Martoanez, A.M. Chaparro and R. Bayoan,“ Photovoltaic Windows By Chemical Bath Deposition,” *Thin Solid Films,* **361**, 28 (2000).

[49] O. Vigil, O.Z. Angel and Y. Rodriguez, “Changes of the Structural and Optical Properties of Cubic CdS Films on Annealing in H_2 and Air Atmospheres,” *Semicond. Sci. Technol.*, **15**, (2000) 259.

[50] H. Metin and R. Esen, “Annealing Studies on CBD Grown CdS Thin Flms,” *J. Cryst. Growth,* **258**, 141 (2003).

[51] S. Soundeswaran, O.S. Kumar and R. Dhanasekaran, “Effect of Ammonium Sulfate on Chemical Bath Deposition of CdS Thin films,” *Mater. Lett.,* **58**, 2381 (2004).

[52] S. Prabahar and M. Dhanam,“ CdS Thin Films from Two Different Chemical Baths-Structural and Optical Analysis,” *J. Cryst. Growth,* **285**, 41 (2005).

[53] J.N.X. Quiebras, G.C. Puente, G.R. Morales, O. Vigila, G.S. Rodriguez and A.M. Acevedo, “Recent Status of Chemical Bath Deposited Metal Chalcogenide and Metal Oxide Thin Films,” *Sol. Energy Mater. Sol. Cells,* **90**, 727 (2006).

[54] D.A.M. Montijo, M.S. Lerma, M.Q. Lopez, M.E. Bouanani, H.N. Alshareef, F.J.E. Beltran and R.R. Bon,“ Recent Status of Chemical Bath Deposited Metal Chalcogenide Thin Films,”*Appl. Surf. Sci.,* **254**, 499 (2007).

[55] M.D. Archbold, D.P. Halliday, K. Durose, T.P.A. Hase, D.S. Boyle, S. Mazzamuto, N. Romeo and A. Bosio,“ Development of Low Temperature Approached to Device Quality CdS: A Modified Geometry for Solution Growth of Thin Films and Their Characterisation,” *Thin Solid Films,* **515**, 2954 (2007).

[56] H. Khallaf, I.O. Oladeji, G. Chai and L.Chow, “Characterization of CdS Thin Films Grown by Chemical Bath Deposition using Four Different Cadmium Sources,” *Thin Solid Films,* **516**, 7306 (2008).

[57] A. G. Pattantyus-Abraham, I. J. Kramer, A. R. Barkhouse, X. Wang, G. Konstantatos, R. Debnath, L. Levina, I. Raabe, M. K. Nazeeruddin and M. Gratzel, "Depleted-Heterojunction Colloidal Quantum Dot Solar Cells," *Acs Nano,* **4**, 3374 (2010)

[58] R. Debnath, J. Tang, D. A. Barkhouse, X. Wang, A. G. Pattantyus-Abraham, L. Brzozowski, L. Levina and E. H. Sargent, "Ambient-Processed Colloidal Quantum Dot Solar Cells via Individual Pre-Encapsulation of Nanoparticles," *J. Am. Chem. Soc.,* **132**, 5952 (2010).

[59] H. Lee, H. C. Leventis, S. J. Moon, P. Chen, S. Ito, S. A. Haque, T. Torres, F. Nüesch, T. Geiger, S. M. Zakeeruddin, M. Gratzel and M. K. Nazeeruddin, "PbS and CdS Quantum Dot-Sensitized Solid-State Solar Cells: "Old Concepts, New Results"," *Adv. Funct. Mater.,* **19**, 2735 (2009).

[60] X. Wang, G. I. Koleilat, J. Tang, H. Liu, I. J. Kramer, R. Debnath, L. Brzozowski, D. A. R. Barkhouse, L. Levina, S. Hoogland and E. H. Sargent, "Tandem Colloidal Quantum Dot Solar Cells Employing a Graded Recombination Layer," *Nat. Photonics,* **5**, 480 (2011).

[61] J. Hernandez-Borja, Y. V. Vorobiev and R. Ramirez-Bon, "Thin Film Solar Cells of CdS/PbS Chemically Deposited by an Ammonia-Free Process," *Sol. Energy Mater. Sol. Cells,* **95**, 1882 (2011).

[62] G. H. Kim, H. B. Kim, B. Walker, H. Choi, C. Yang, J. Park and J. Y. Kim, "Effects of Ionic Liquid Molecules in Hybrid PbS Quantum Dot-Organic Solar Cells," *ACS Appl. Mater. Interfaces,* **5**, 1757 (2013).

[63] Z. Liu, J. Han, L. Han, K. Guo, Y. Li, T. Cui, B. Wang and X. Liang, "Fabrication of ZnO/CuS Core/Shell Nanoarrays for Inorganic–Organic Heterojunction Solar Cells," *Mater. Chem. Phys.,* **141**, 804 (2013).

[64] B. Ghosh, M. Das, P. Banerjee and S. Das, "Fabrication and Optical Properties of SnS Thin Films by SILAR Method," *Appl. Surf. Sci.,* **254**, 6436 (2008).

[65] K. Ramakrishna Reddy, P. Purandhara Reddy, P. Datta and R. Miles, "Formation of Polycrystalline SnS Layers by a Two-Step Process," *Thin Solid Films,* **403**, 116 (2002).

[66] J. Johnson, H. Jones, B. Latham, J. Parker, R. Engelken and C. Barber, "Optimization of Photoconductivity in Vacuum-Evaporated Tin Sulfide Thin Films," *Semicond. Sci. Technol.,* **14**, 501 (1999).

[67] S. Hegde, A. Kunjomana, K. Chandrasekharan, K. Ramesh and M. Prashantha, "Optical and Electrical properties of SnS Semiconductor Crystals Grown by Physical Vapor Deposition Technique," *Physica B,* **406**, 1143 (2011).

[68] C. Cifuentes, M. Botero, E. Romero, C. Calderon and G. Gordillo, "Optical and Structural Studies on SnS Films Grown by Co-Evaporation," *Braz. J. Phys.,* **36**, 1046 (2006).

[69] H. Moreno-Garcia, M.T.S. Nair and P.K. Nair, "All-Chemically Deposited Bi_2S_3/PbS Solar Cells," *Thin Solid Films,* **519**, 7364 (2011).

[70] H. Borja, Y .V. Vorobievn, and R. Ramirez-Bon, "Thin Film Solar Cells of CdS/PbS Chemically Deposited by an Ammonia-Free Process", *Solar Energy Materials & Solar Cells,* **95**, 1882 (2011).

[71] A. S. Obaid, Z. Hassan, M. A. Mahdi and M. Bououdina,"Fabrication and Characterization of n-CdS/p-PbS Heterojunction Solar Cells Using Microwave-Assisted Chemical Bath Deposition," Solar Energy, **89**,143 (2013).

[72] S. Messina, M T S Nair and P K Nair, "Antimony sulphide thin film as an absorber in chemically deposited solar cells", J. Phys. D: Appl. Phys., **41,** (2008) 095112.

[73] K. P. Bhandari, P. J. Roland, H. Mahabaduge, N. O. Haugen, C. R. Grice, S. Jeong, T. Dykstra, J. Gao and R. J. Ellingson, "Thin Film Solar Cells Based on the Heterojunction of Colloidal PbS Quantum Dots With CdS," *Sol. Energy Mater. Sol. Cells,* **117**, 476 (2013).

[74] S. Ramprasad, Y.W. Su, C. Chang, B. K. Paul and D. R. Palo, "Cadmium Sulfide Thin Film Deposition: A Parametric Study Using Microreactor-Assisted Chemical Solution Deposition," *Sol. Energy Mater. Sol. Cells,* **96**, 77 (2012).

[75] S. Sartale and C. Lokhande, "Growth of Copper Sulphide Thin Films by Successive Ionic
Layer Adsorption and Reaction (SILAR) Method," *Mater. Chem. Phys.,* **65**, 63 (2000).

[76] D. Saikia, P.K. Gogoi and P.K. Saikia," Fabrication and Evaluation of CdS/PbS Thin Film Solar Cell by Chemical Bath Deposition Technique," *Chalcogenide Lett.*, **5**, 317 (2010).

[77] S. Messina, M. Nair and P. Nair, "Antimony Selenide Absorber Thin Films in All-Chemically Deposited Solar Cells," *J. Electrochem. Soc.,* **156**, 327 (2009).

[78] V. Popescu, H. I. Nas-cu and E. Darvasi," Optical Properties of PbS-CdS Multilayers and Mixed Thin Films Deposited on Glass Substrate by Spray Pyrolysis," *J. of Optoelec. and Advanced Mater.*, **8**, 118 (2006).

[79] S. Prabaha, N. Suryanaranyanan, K. Rajasekar and S. Srikanth," Lead Selenide Thin Films from Vaccum Evaporation Method- Structural and Optical Properties," *Chalcogenide Letters*, **6**, 204 (2009).

[80] M. Farady, A. I. Hochbaum, J. Goldberger, M. Zhang and P. Tang," Synthesis and Thermoelectrical Characterization of Lead Chalcogenide Nanowires," *Advanced Materials*, **19**, 3047 (2007).

[81] J. Aguilar-Hernandez," Photoluminescence and Structural Properties of Cadmium Sulfide Thin Films Grown by Different Techniques," *Semicond. Sci. Technol.,* **18**, 111 (2003).

[82] E. Pentia, L. Pintilie, I. Matei, T. Botila and E. Ozbay," Chemically Prepared Nanocrystalline PbS Thin Films," *J. of Optoele. and Advanced Mater.*, **3**, 525 (2001).

[83] B. D. Cullity," Elements of X-ray diffraction," *Second Edn., Addison-Wesley, Massachusetts*, (1978).

[84] I. M. Watt," The principles and practice of electron microscopy," *Cambridge University Press, Cambridge* (1983).

[85] P. J. Goodhew, J. Humphreys and R. Beanland," Electron Microscopy and Analysis," *Taylor Francis, London*, (2000).

[86] K. S. Birdi," Scanning Probe Microscopes: Applications in Science and Technology," *CRC Press, Boca Raton* (2003).

[87] E. Meyer, H. J. Hug and R. Bennewitz," Scanning Probe Microscopy: The Lab on a Tip," *Springer- Verlag Berlin* (2004).

[88] S. Morita, R. Wiesendanger and E. Meyer," Noncontact Atomic Force Microscopy," *Springer: Berlin* (2002).

[89] A. Mehta," UV-Vis Spectroscopy- Limitations and Deviations of Beer- Lambert Law," *Analytical Chemistry* (2012).

[90] P. Misra and M. A. Dubinskii," Ultraviolet Spectroscopy and Uv- Lasers," *New York, Marcel Dekker* (2002).

[91] B. W. Kempshall, L. A. Giannuzzi, B. I. Prenitzer, F. A. Stevie and S. X. Da," Comparative Evaluation of Protective Coatings and Focused Ion Beam Chemical Vapor Deposition Processes," *Journal of Vacuum Science & Technology B:Microelec- tronics and Nanometer Structures,* **20**, 286 (2002).

[92] A. L. Patterson," The Scherrer Formula for X- Ray Particle Size Determination," *Phys. Rev.*, **56**, 978 (1939).

[93] M. A. Rafea and N. Roushdy," Study of Optical Properties of Nanostructured PbS Films," *Philosophical Magazine Letters,* **90**, 113 (2010).

[94] O. Zelaya-Angel, J.J. Alvarado-Gil, R. Lozada-Morales, H. Varges and A. Ferreira da Silva," Band-Gap Shift in CdS Semiconductor by Photo acoustic Spectroscopy: Evidence of a Cubic to Hexagonal Lattice Transition," *Appl. Phys. Lett.,* **64**, 291 (1994).

[95] M. Rusu, A. Rumberg, S. Schuler, S. Nishiwaki, R. Wurz, S.M. Babu, M. Dziedzina, C. Kelch, S. Siebentritt, R. Klenk, Th. Schedel-Niedrig and M.Ch. Lux-Steiner,"

Optimisation of the CBD CdS Deposition Parameters for ZnO/CdS/CuGaSe Solar Cells," *Journal of Physics and Chemistry of Solids*, **64**,1849 (2003).